Hygroscopic properties and mixing state of aerosol measured at the high altitude site Puy de Dôme (1465 m a.s.l.), France

H. Holmgren, K. Sellegri, M. Hervo, C. Rose, E. Freney, P. Villani* and P. Laj**

Laboratoire de Météorologie Physique, CNRS UMR6016, Observatoire de Physique du Globe de Clermont-Ferrand, Aubière Cedex, Université Blaise Pascal, France

* now at Soluzioni e Sviluppo Strumentazione Scientifica, Modena, Italy

** now at Laboratoire de Glaciologie et Géophysique de l'Environnement, CNRS UMR5183, Université Joseph Fourier Grenoble 1, St Martin d'Hère, France

Correspondence to: K. Sellegri (k.sellegri@opgc.cnrs.fr)

Abstract

A hygroscopicity tandem differential mobility analyzer (HTDMA) was used to evaluate the hygroscopic properties of aerosol particles measured at the Puy de Dôme research station in central France, periodically from September 2008 to January 2010, and almost continuously from October 2010 to December 2012. This high-altitude site is ideally situated to allow for both the upper part of the planetary boundary layer and the lower free troposphere to be sampled. The aim of the study is to investigate both the influence of year-to-year, seasonal, and diurnal cycles, as well as the influence of air mass type on particle hygroscopicity and mixing state.

Results show that particle hygroscopicity increases with particle size and depends both on air mass type and on season. Average growth factor values, GFs, are lowest in winter (1.21±0.13, 1.23±0.18 and 1.38±0.25 for 25, 50 and 165 nm particles, respectively) and highest in autumn (1.27±0.11, 1.32±0.12 and 1.49±0.15 for 25, 50 and 165 nm particles, respectively). Particles are generally more hygroscopic at night than during the day. The seasonal and diurnal variations are likely to be strongly influenced by boundary layer dynamics. Furthermore, particles originating from oceanic and continental regions tend to be more hygroscopic than

those measured in African and local air masses. The high hygroscopicity of oceanic aerosol can be explained by large proportions of inorganic aerosol and sea salts.

Aerosol measured at the Puy de Dôme display a high degree of external mixing, and hygroscopic growth spectra can be divided into three different hygroscopic modes: a less hygroscopic mode (GF < 1.3), a hygroscopic mode (GF 1.3-1.7) and a more hygroscopic mode (GF > 1.7). The majority of particles measured can be classified as being in either the less hygroscopic mode or the hygroscopic mode, and only few of them have more hygroscopic properties. The degree of external mixing, evaluated as the fraction of time when the aerosol is found with two or more aerosol populations with different hygroscopic properties, increases with particle size (average yearly values are 20, 28 and 45% for 25, 50, and 165 nm particles, respectively). The degree of external mixing is more sensitive to season than to air mass type, and it is higher in the cold seasons than in the warm seasons.

With more than two years of nearly continuous measurements, this study gathers the results from one of the longest data sets of hygroscopic growth factor measurements to date, allowing a statistically relevant hygroscopic growth parameterization to be determined as a function of both air mass type and season.

1 Introduction

Atmospheric aerosol particles affect the Earth's climate in various ways. As a direct effect, they scatter and absorb solar radiation. In addition, some aerosols can be activated to form cloud droplets, and will thereby indirectly impact the radiation budget of the planet. The impacts of aerosol particles on the climate are subject to many uncertainties, which are linked to their physical and chemical properties (IPCC, 2013). Both the direct and indirect effect on radiation is influenced by aerosol particle hygroscopicity, meaning that hygroscopicity is a key parameter to better understand and estimate aerosol radiative impacts and aerosol-cloud interactions. Chemical compounds may be present in aerosol particles as internal mixtures (all particles of a given size have the same chemical composition), or external mixtures (particles of a given size are divided into several sub-populations of different chemical composition). The mixing state of the aerosol particles may have an impact on the way they interact with water vapour (i.e. on their indirect effect), and on the way they interact with solar radiation (i.e. on their direct effect).

Hygroscopic properties and mixing state of atmospheric aerosol particles can be studied in detail using a Hygroscopicity Tandem Differential Mobility Analyzer (HTDMA). This

instrument selects a narrow range of particle diameters (D_0) from a polydisperse aerosol, and exposes the selected particles to a well defined elevated relative humidity, which is normally 90% (RH90). Due to water uptake, the diameter of the selected particles will increase (D_{90}), and a hygroscopic growth factor (GF) can be calculated. The mixing state of aerosol particles can be evaluated from hygroscopicity measurements, when a population of particles selected at a given diameter falls into different hygroscopic modes, pointing to the presence of different aerosol populations for this size.

An overview of HTDMA data on atmospheric aerosol reported up to September 2007 has been summarized in a review article by Swietlicki et al. (2008). Historically, most data have been obtained during intensive field campaigns, covering only a few weeks to some months of measurements. Marine, rural, and urban environments have been studied rather extensively over the last 20 years (see e.g. Swietlicki et al. (2008) and references therein), while measurements at high altitude sites, i.e. away from local sources and periodically in the free troposphere (FT), are more rare. Measurements at high altitude sites are important when considering the climatic effect of tropospheric clouds, which are largely formed on FT aerosol. For the formation of convective clouds (e.g., cumulus), boundary layer (BL) aerosols also play an important role. Up until now, HTDMA measurements at high altitude sites have been studied at the research station Jungfraujoch in the Swiss Alps (3580 m a.s.l.) (Weingartner et al. 2002; Sjögren et al. 2008; Kammermann et al. 2010), the Izaña baseline observatory station on the island of Tenerife in the north-eastern Atlantic (2367 m a.s.l.) (Swietlicki et al. 2000), and the Monte Cimone observatory in northern Italy (2165 m a.s.l.) (Van Dingenen et al. 2005).

The Puy de Dôme research station (pdD) in central France is ideally situated for measurements of various types of air masses. Located at 1465 m a.s.l. it lies in a region which allows for both the upper part of the planetary boundary layer (PBL) and the lower part of the FT to be sampled, depending on meteorological conditions. In this study, the aim is to investigate aerosol hygroscopic properties and aerosol particle mixing state, away from direct sources at a background site. The work presented covers data collected in periods from September 2008 to January 2010, and almost continuously from October 2010 to December 2012. This is, to the authors' knowledge, the first study that investigates hygroscopic properties of particles measured at a high altitude site almost continuously over more than two

years. This allows for detailed analysis of the influence of year-to-year and seasonal cycles, diurnal patterns, and air mass types on particle hygroscopicity.

2 Methods

2.1 Measurement site

The Puy de Dôme research station (pdD) is located at the top of Puy de Dôme, 1465 m a.s.l. in central France (45°46'N, 2°57'E), 16 km west of the city of Clermont-Ferrand (396 m a.s.l., about 140 000 inhabitants). The site has been defined as a rural background site (Putaud et al. 2004) and as a high altitude site (Asmi et al. 2011). According to Henne et al. (2010), the site is representative of western European air masses over a large scale. The station surrounding area is mainly dominated by fields and forests. Meteorological parameters such as wind speed and direction, temperature, relative humidity, radiation (global, UV and diffuse), atmospheric trace gases (O_3, NO_X, SO_2, CO_2), particulate black carbon (BC), and aerosol particle number concentration are monitored continuously. The site is often used for investigations of cloud microphysical properties, cloud chemistry and aerosol-cloud interactions (Wobrock et al, 2001; Sellegri et al. 2003; Marinoni et al. 2004, Asmi et al., 2012), due to frequent formation of clouds (>50% of the time from November to March). Boundary layer heights (BLH) over several seasons have been calculated from model outputs (Venzac et al. 2009) or retrieved from remote sensing measurements (Boulon et al. 2011). BLH retrievals were cross-checked using meteorological parameters (Boulon et al. 2011) and in situ aerosol measurements (Venzac et al. 2009). Both studies indicate that in winter, spring, and at night during summer, the site is more often influenced by FT or residual layer (RL) air masses, compared to the summer season (Venzac et al. 2009; Boulon et al., 2011).

2.2 Instrumentation

The Hygroscopicity Tandem Differential Mobility Analyzer (HTDMA) system used in this study is designed and built at the Laboratoire de Météorologie Physique (LaMP). The instrument includes silica gel dryers, two Differential Mobility Analyzers (DMAs), a humidifying section, and a Condensation Particle Counter (CPC). First, a polydisperse aerosol is sampled at a flow rate of about 0.6 l/min. This aerosol is dried to less than 30% RH, using silica gel diffusion driers. The first DMA (DMA1) alternatively selects six different dry diameters (D_0) from the polydisperse aerosol: 25, 35, 50, 75, 110 and 165 nm. Selected

particles are subsequently exposed to 90% RH, using a humidification system. The humidification system consists of a nafion membrane exposed to humid air generated by bubbling the air through distilled water (18 Ohm). RH is measured and controlled by a dew point mirror placed on the second DMA (DMA2) sheath loop. The particle diameter increases as a result of water uptake, and the resulting particle size (D_{90}) is measured with DMA2, while the particle concentration is measured by the CPC. The ratio of D_{90} to D_0 is defined as the hygroscopic growth factor (GF). The particle concentration measured by the CPC as a function of GF is referred to as the measurement distribution function (MDF). An MDF covering the whole GF range can be obtained by changing the diameter selected by DMA2 gradually or in discrete steps, while keeping DMA1 at a constant dry size. The first and the second DMA are operated using a closed-loop/vacuum pump set-up. A critical orifice and mass flow controllers are used to control the sheath aerosol flow rate at 3 l/min. The system is confined and cooled by Peltier systems (ΔT close to ±5°C).

The accuracy of the RH sensors of the HTDMA at the pdD is regularly checked using pure ammonium sulphate, which has a well known GF value at 90% RH. Intercomparisons performed during a EUSAAR workshop (Duplissy et al. 2009) showed that the average variability of measurements compared with other HTDMA instruments is less than 1%. The humidification system presented a stability of ±3% RH in normal conditions.

2.3 Analysis

2.3.1 Data inversion and fitting procedure

In this work, growth factor probability density functions (GF-PDFs) are obtained from the measured GFs following the procedures given by Gysel et al. (2009). The method uses a full TDMA transfer forward function in combination with a χ^2 minimization algorithm, which has been tested on HTDMA data (Gysel et al. 2007; Allan et al. 2008). A piecewise linear inversion approach was used, with the center of the first and the last inversion bins set to GF=0.7 and GF=2.5, respectively. The resolution chosen was ΔGF = 0.15. All GF-PDFs measured in the range 87% < RH < 93% were recalculated to RH=90% according to equations (3) and (6) in Gysel et al. (2009). Data acquired at lower or higher RH were ignored and scans that show particle counts less than 1 cm^{-3} are not included in the analysis.

The HTDMA at the pdD is calibrated using ammonium sulphate, which has well documented hygroscopic parameters. With a resolution ΔGF = 0.15 chosen for the fit, the spread in data

obtained by ammonium sulphate is $\sigma < 0.05$. According to Sjögren et al. (2008), GF-PDFs showing $\sigma \leq 0.10$ indicate an internal mixture, or a quasi-internal mixture with limited spread of growth modes. Contrary, GF-PDFs with $\sigma \geq 0.15$ are considered externally mixed, or quasi-internally mixed with substantial spread of growth factors. These mixing state criteria were followed to evaluate data also in this work.

Hygroscopic growth factor distributions are quite complex at the pdD, often with two and sometimes three hygroscopic modes observed simultaneously. This indicates a high degree of external mixing and the influence of multiple sources of particles at the site. When the distribution is multi-modal, the average GF provided by the TDMAinv program is not sufficient to fully describe the different hygroscopic modes of individual GF-PDFs. All data is therefore further interpreted using a Matlab program developed at LaMP. By describing the obtained GF-PDF as a superposition of multiple Gaussians, the growth factor GF, spread σ, and number fraction NF of particles in each hygroscopic mode can be identified for every scan individually. This means that when the GF spread in the DMA transfer is higher than expected ($\sigma > 0.10$), two different hygroscopic modes are searched to explain this spread. The aspect of this type of analysis, with a strict mode fitting procedure for each individual GF-PDF, enables a more accurate idea of the aerosol mixing state. Figure 1 is an example of a bimodal growth factor distribution obtained from the TDMAinv program, where the software provides an average GF of 1.38 and a spread σ of 0.18. The different modes are identified using the Matlab program and a fit of multiple Gaussians on a single GF spectrum analysis. In this example, a first GF mode is identified at GF 1.00 and σ 0.07 and a second at GF 1.37 and σ 0.09.

Further, hygroscopic kappa values κ, as introduced by Petters and Kreidenweis (2007), are calculated according to Eq. (1)

$$\kappa = \frac{(GF^3-1)(1-a_w)}{a_w}, \quad (1)$$

where a_w is the water activity, at which the GF was measured. According to Köhler theory (Köhler, 1936), a_w is obtained by Eq. (2)

$$a_w = \frac{RH}{\exp\left(\frac{4\sigma_{sv_w}}{RTD}\right)}, \quad (2)$$

where σ_s is the surface tension of the solution droplet (here assumed to be pure water), v_w is the partial molar volume of water in solution, R is the universal gas constant, T is the temperature, and D is the diameter of the droplet.

2.3.2 Air mass back trajectory calculations

Back trajectories for air masses arriving at the pdD were calculated using HYSPLIT (HYbrid Single-Particle Lagrangian Integrated Trajectory) (Draxler and Hess, 1998). Trajectories were calculated for the arrival pressure 850 hPa at the height of the pdD every 6 hours, going back 72 hours in time, and were classified as continental, African, oceanic or oceanic modified as seen in Figure 8 (sectors: 10-130, 130-260, 260-315 and 315-10, respectively, according to Asmi et el. 2012). The classification oceanic modified refers to air masses originating from the ocean, which have traveled over the continent and are thus influenced by continental sources. In addition, air masses predominantly circulating above continental France were classified as local.

3 Results and discussion

In the first stage of data analysis, the general behavior of the hygroscopic properties of particles is studied as a function of all sampled particle sizes (25, 35, 50, 75, 110 and 165 nm). Then, focus is put on the analysis of the hygroscopic growth and mixing state of particles with dry sizes 25, 50 and 165 nm. These sizes of aerosol particles are representative of the nucleation mode (25 nm), the Aitken mode (50 nm), and the accumulation mode (165 nm) at the pdD (Venzac et al. 2009). Table S1 in the Supplement gives the total number of successful scans for each particle size, split by calendar month.

Based on literature, black carbon (BC) and mineral dust can be considered almost hydrophobic with a GF less than 1.05 (Weingartner et al. 1997; Vlasenko et al. 2005), while biomass burning aerosols can have a wide range of GFs increasing up to 1.65 (Cocker et al. 2001; Pagels et al. 2003). These very high values were measured after the biomass burning particles have had some time to mix with secondary inorganic ions, and much lower GFs were measured closer to the source. The main inorganic ions (NO_3, SO_4 and NH_4) can be associated with ammonium sulphate or ammonium nitrate, which have GFs around 1.7 (Gysel et al. 2002; Prenni et al. 2003; Wise et al. 2003). GFs of secondary organic aerosol (SOA) range between 1.07 and 1.14 (Virkkula et al., 1999; Saathoff et al.; 2003; Baltensperger et al., 2005) and up to more than 1.65 for aged SOA in simulation chamber studies (Duplissy et al.,

2011). The GFs of organic compounds may vary between about 1.0 and 1.7. (Peng et al., 2001; Wise et al., 2003; Chan and Chan, 2003; Prenni et al., 2003, 2007; Koehler et al., 2006; Huff Hartz et al., 2006). The terpenes α-pinene and β-pinene have been reported to have GFs between about 1.03 and 1.18 (Saathoff et al. 2003; Varutbangkul et al. 2006; Prenni et al. 2007). Finally, particles composed of sea salt or sulphuric acid are very hygroscopic with GFs higher than 2.0 (Gysel et al. 2002; Koehler et al. 2006).

3.1. Year-to-year and seasonal variability

In order to provide an overview of particle hygroscopicity, average GF-PDFs were calculated for each continuous measurement year (2011 and 2012). As observed in several studies (see e.g. Swietlicki et al. (2008) and references therein), there is a distinct increase in hygroscopicity with increasing particle diameter (Figure 2a). Nucleation mode particles have average GF values of around 1.1-1.2, while particles in the Aitken mode cover a larger range of GFs and show more variability than those in the nucleation mode. In 2011, the GF peaks at around 1.1, and in 2012 it has increased to about 1.2. Finally, accumulation mode particles cover GFs from less than 1.0 to over 2.2 and show more variability between 2011 and 2012. In the accumulation mode, the GF-PDF is often bimodal with a first mode located close to 1.0 and a second mode between 1.4 and 1.6.

The size dependent hygroscopicity solely due to the aerosol composition can be addressed by plotting κ-PDFs as a function of particle diameter, calculated for 25, 35, 50, 75, 110 and 165 nm (Figure 2b) using the hygroscopicity distribution concept as described by Su et al. (2010). Both in 2011 and 2012, the aerosol hygroscopicity is increasing with increasing particle size independently of the Kelvin effect from 50 nm to larger sizes. There is also a tendency of the nucleation mode particles to be slightly more hygroscopic than the Aitken mode particles. Years 2011 and 2012 are on average very similar, with more dispersion in the hygroscopicity of the accumulation mode particles during 2012.

Seasonal variations in particle hygroscopicity were assessed using data from 2008, 2009, 2010, 2011 and 2012. In 2008, data was only collected in September, while 2009 includes winter and spring time measurements. In 2010, winter and autumn are represented, but neither spring nor summer. In 2011 and 2012, measurements took place over all seasons. Winter at the pdD stretches from December to February, spring from March to May, summer from June to August and autumn from September to November.

Monthly median hygroscopic GFs and κ values were calculated from the GF-PDFS and are displayed in Figure 3, while Table 1 gives seasonal averages. Figure 3 shows that aerosol hygroscopicity is lower in winter than during summer. It is also observed, from the large error bars, that the variability is higher in winter than in summer. Particles in the nucleation mode do not show any strong seasonal variability, as the average GF is roughly constant throughout the year. Aitken and accumulation mode particles are generally most hygroscopic in autumn and least hygroscopic in winter.

Weingartner et al. (2002), Sjögren et al. (2008), and Kammermann et al. (2010) studied hygroscopic properties at the FT site Jungfraujoch (JFJ) in the Swiss Alps (3580 m a.s.l.). In the first two studies GFs were measured at 85% RH, but could be extrapolated to 90% RH. In winter, when the JFJ site is predominantly influenced by lower FT air masses, Weingartner et al. (2002) reported GFs of 1.55 and 1.62 for 50 and 100 nm particles, respectively. Later, Sjögren et al. (2008) measured winter time GFs to be 1.45 for 50 nm particles and 1.60 for 100 nm particles. These authors also measured particle hygroscopicity in summer time, when the sampled air can be influenced by injections from the PBL, giving calculated GFs (RH90) of 1.35 and 1.40 for 50 nm and 100 nm particles, respectively. Finally, Kammermann et al. (2010) evaluated JFJ hygroscopicity data over 13 months and found the yearly average GFs to be 1.34 and 1.43 for 50 and 110 nm particles, respectively. They found no distinct seasonal variability in the values measured. The reported winter time GFs were 1.30 for 50 nm particles and 1.41 for 110 nm particles, and the corresponding summer time values were 1.34 and 1.40. GF spectra measured at Monte Cimone (Van Dingenen et al. 2005) and Izaña (Swietlicki et al. 2000), which have large contributions of anthropogenic emissions, were reported to be bimodal, and no average GFs were presented.

GFs reported from JFJ are compared to those measured in this study in Table 2. The yearly averages measured by Kammermann et al. (2010) are close to those observed at the pdD. This is also the case for the summer time values given by Sjögren et al. (2008) and Kammermann et al. (2010). However, winter time GFs measured by Weingartner et al. (2002) and Sjögren et al. (2008) are much higher than those observed in this work, while those given by Kammermann et al. (2010) are more similar. Overall, GFs measured at JFJ are generally higher than those measured at the pdD. A likely explanation to this could be that the JFJ site is located at a higher altitude than the pdD station, and is thus less influenced by the advection of pollution aerosols from the PBL. Indeed, opposite to observations at the pdD,

Kammermann et al. (2010) found that PBL influence has no effect on the annual mean hygroscopicity of the aerosol measured at JFJ, although GFs are significantly lowered during the short periods with PBL influence.

GF-PDFs measured at the pdD were averaged over each season in Figure 4a. For particles in the nucleation mode, the shape of the GF-PDF is similar for all seasons, peaking between 1.1 and 1.2. Aitken mode particles are characterized by a wide range of GFs, especially in the cold seasons. The distribution function peaks at a lower GF in winter and in summer (GF peaks at about 1.1) than during other seasons (GF peak 1.1-1.3). For accumulation mode particles, the shape of the GF-PDF strongly depends on the season. In winter and in autumn two modes are clearly visible, with a first mode located between 1.0 and 1.1 and a second mode around 1.5-1.6. The occurrence of this nearly hydrophobic mode in winter lowers the average GF as reported in Table 1. The very low GF values observed here point to either BC-rich biomass burning aerosol or BC-rich particles associated with other combustion sources, such as fossil fuel combustion aerosol, which have had little time to mix with secondary inorganic ions.

Again, the hygroscopic properties of aerosol solely due to their chemical composition can be investigated using the κ-PDF as a function of particle size. Figure 4b indicates that the higher hygroscopicity of nucleation mode particles relative to the Aitken mode particles observed on the yearly average is mainly seen in autumn and winter. Otherwise the particle hygroscopicity, as well as the external mixing degree, is increasing with particle size for all seasons. The appearance of a more hygroscopic and a less hygroscopic mode at larger particle sizes is mainly observed during autumn and winter.

The observation of several hygroscopic modes in the GF-PDFs measured at the pdD indicates a high degree of external mixing that needs to be characterized. Each of the individually retrieved GF-PDFs was examined in more detailed using the Gaussian fitting procedure described in section 2.3.1. Briefly, when the spread in a single GF-PDF was greater than $\sigma > 0.10$, two different hygroscopic modes were searched to explain this spread. This procedure allowed identification of several hygroscopic modes with a specific median growth factor GF, GF spread (σ) and number fraction NF found in each mode. The calculated median GF of each mode was then attributed to one of three hygroscopic classes. Mode 1 represents less hygroscopic material with GFs lower than 1.3, i.e. black carbon and organic material. Mode 2 corresponds to hygroscopic particles with GFs between about 1.3 and 1.7, e.g. ammonium

sulphate and mixtures of ammonium sulphate and organic material. Mode 3 is the more hygroscopic mode, with GFs higher than 1.7. These are particles most likely composed of sea salt and modified sea salt. Modified sea salt refers to sea salt that has been modified by other species in the air, for example condensation of secondary continental species. It should also be mentioned that particles with relatively high GF values may still contain BC if the inorganic ion volume fraction is very high; it is not possible to assess whether a small BC core is present using this method. Table 3 gives the average GF of each hygroscopic mode and the frequency of occurrence (FO) of that mode, i.e. the fraction of scans in which you find particles in mode 1, mode 2 or mode 3, respectively. The data shows that the less hygroscopic mode (mode 1) is most important for nucleation and Aitken mode particles, occurring in 86 and 84% of all scans, respectively. For accumulation mode particles, the hygroscopic mode (mode 2) is strongest, with a FO of 79%. The average GFs of each hygroscopic mode (GF1, GF2, GF3) are roughly the same for all particle sizes; only the FO changes.

Table 4 shows the frequency of external mixing split by season, i.e., the percentage of scans that display two or more modes. At the pdD, the aerosol is found as an external mixture from 16 to 67% of the time, depending on both particle size and season. It is clear that the degree of external mixing increases with particle size, and that it is higher in the cold seasons than in the warm seasons. During winter, the boundary layer height is more frequently at the height of puy de Dome, so that aerosol measurements are made at the interface between the PBL and the FT. Therefore during the winter months, the change in aerosol sources results in a large variation in GF values.

Sjögren et al. (2008) used the GF spread (σ) for individual scans to conclude that winter time aerosol measured at JFJ is predominantly internally mixed. Nonetheless, the authors' did find a small GF mode at about 1.0-1.2, in addition to the main mode. The mode was less pronounced for 50 nm particles than for 100 nm particles, which is coherent with the trend of the degree of mixing with particle size seen at the pdD. Similar to the pdD, the JFJ summer time aerosol showed a more homogeneous distribution. Kammermann et al. (2010) also found that 50 nm particles were characterized by a broad peak including the full range of particle compositions. Particles larger than 75 nm were more clearly bi-modal, again in agreement with the pdD trend showing a higher degree of mixing with larger particle size.

Monthly average GFs and NFs of particles in each hygroscopic mode, measured at the pdD, are displayed in Figure 5. Overall, less hygroscopic particles are dominating in winter time,

but their relative number fraction (NF1) decreases as spring arrives and the number fraction of hygroscopic particles (NF2) increases. The nucleation mode is dominated by less hygroscopic particles throughout the whole year (NF1: 57-88%), although the hygroscopic mode contributes significantly (NF2: 11-43%). More hygroscopic particles are present only at very low number fractions (NF3: < 1%). The Aitken mode mostly contains less hygroscopic and hygroscopic particles. Hygroscopicity is lowest in winter (NF1: 61-79%, NF2: 20-34%, NF3: < 5%) and highest from late spring to early autumn (NF1: 39-56% NF2: 21-59%, NF3: < 2%). The accumulation mode is most sensitive to seasonal variations. The less hygroscopic mode is dominant only during winter months (NF1: 43-63%, NF2: 28-47%, NF3: 3-24%). As spring arrives, this fraction decreases (NF1: < 38%) and the hygroscopic fraction increases (NF2: 51-83%). In autumn, the less hygroscopic fraction slowly begins to increase again. The more hygroscopic mode only contributes low number fractions throughout the year (NF3: 5-10%), with a maximum fraction present during winter. This observation is in agreement with a more efficient long-range transport of sea salt particles to the site in winter (Bourcier et al. 2012). Figure 5 also shows that for nucleation and Aitken mode particles the average GF in the less hygroscopic mode (GF1) increases in the warm season, while the GF of hygroscopic mode (GF2) and the more hygroscopic mode (GF3) remains more or less the same. In the accumulation mode, GF1, GF2 and GF3 show no significant variation throughout the year.

Freney et al. (2011) suggest that low volatility oxygenated organic aerosol particles (LV-OOA) measured at the pdD in winter are related to aged biomass burning emissions, whereas organic aerosol particles measured in summer are linked to biogenic sources. The hygroscopicity of particles originating from biomass burning can vary significantly (Pagels et al. 2003), but they are globally less hygroscopic than organic particles originating from biogenic sources. This change of organic sources from winter to summer would explain the increase in GF1 from winter to summer in the nucleation and Aitken modes. Bourcier et al. (2012) and Freney et al. (2011) found that the fraction of black carbon (BC) measured at the pdD is low (< 5%), while the organic fraction, which could also contribute to the number fraction of less hygroscopic particles, varies between 23% (Freney et al. 2011) and 48% (Bourcier et al. 2012) in winter. In summer, the organic fraction contributes to at least 55% (both studies) to the total mass concentration. Thus, it seems like the organic fraction is only variable in winter time, leading to variable values of hygroscopicity. In winter, the PBL height is close to the pdD height during daytime, meaning that the pdD site can be either in the PBL or in the FT. Furthermore, higher fractions of biomass burning aerosol have been

identified at the site during (Crippa et al., 2014). Asmi et al. (2012) measured aerosol cloud activation at the pdD and report that aerosol properties, and likely also their sources, are different between summer and winter. During summer, the authors measured less aged organics, possibly from biogenic sources. Winter time organics had a higher organic aerosol m/z ratio to total organics (f44), suggesting more aged organics.

The seasonal variations of the contribution of different hygroscopic fractions are likely linked to both the seasonal variation of the vertical transport of air masses from the PBL to the pdD site and to seasonal changes in aerosol composition. This vertical transport may also be discussed in the light of the diurnal variations of the hygroscopic fractions in the aerosol.

3.1 Diurnal variability

Particles measured at the pdD show a clear diurnal variation, with a higher GF measured at night time than during the day, as illustrated in Figure 6. For all particle sizes, the median GF is highest in late night/early morning, and lowest around midday. This diurnal variation is due to the less hygroscopic fraction that increases during the day, while the hygroscopic fraction decreases. It is likely the result of the site being in the RL or FT at night, hence being exposed to long-range transport and aged aerosol particles. During the day, there are more air masses arriving from the PBL with a larger contribution from anthropogenic emissions that are less hygroscopic. It is also possible that the partitioning of nitrate or ammonium nitrate at lower temperatures contribute to the higher GF values at night. The diurnal variation is most pronounced for nucleation mode particles.

Nucleation and Aitken mode particles may originate from anthropogenic emissions transported from the PBL or from new particle formation and growth occurring at the site. New particle formation (NPF) events are frequently observed at the pdD during the day (Venzac et al. 2007; Boulon et al. 2011; Rose et al. 2013). Boulon et al. (2011) and Rose et al. (2013) suggest that the nucleated particles grow from condensation of organic compounds, which are likely less hygroscopic. Thus, NPF events will lead to an increase in the less hygroscopic fraction, which could explain the observed diurnal variations at the site.

Hygroscopicity data are further segregated into night (00:00-06:00 UTC) and day (09:00-15:00 UTC), and are split into seasonal averages in Figure 7. The diurnal changes are observable over all seasons and all partice sizes. In winter, the day time increase in the number fraction of less hygroscopic particles (NF1) is smaller than during the other seasons.

This is consistent with observations by Rose et al. (2013), who report that NPF events are less frequent in winter (NPF event frequency 17%) than in spring, summer and autumn (NPF event frequency 26%, 27% and 24%, respectively).

3.2 Influence of air mass origin

Air masses were sorted according to their origin in order to investigate the influence of long range transport on the aerosol hygroscopic behavior measured at the top of the pdD. Back trajectories were calculated from the HYSPLIT model (Draxler and Hess, 1998) every 6 hours, going back 72 hours in time, and were classified as either continental, African, oceanic, oceanic modified or local according to the boundaries defined in Figure 8. The colour coding represents the number of back trajectories arriving at the pdD with a 1°x1° resolution over the measurement period September 2008 – December 2012. The origin of a back trajectory is defined as a function of the number of hours spent over each sector by an air mass. Hygroscopicity data treated in this work arrived from air masses that were 36% oceanic, 29% African, 19% continental, 10% oceanic modified and 6% local. Figure 9 shows that there is a seasonal variation in the frequency of continental air masses. For example, the contribution of continental air is substantial throughout most of the year, but in July and August those air masses are rarely present. Local air masses are most frequent from late spring to early autumn. This is in agreement with the observation of a higher PBL in the warm seasons, in which the winds are weaker.

Table 5 shows the frequency of external mixing split by air mass origin, i.e. the percentage of scans that display two or more modes simultaneously. Particles in the nucleation and Aitken mode have the highest degree of external mixing for oceanic and oceanic modified air masses (21-39%) and the lowest for local air masses (14-20%). Accumulation mode particles show different behaviour, with the degree of external mixing being highest for continental air masses (54%) and lowest for oceanic and oceanic modified air masses (40-42%). The degree of external mixing is less sensitive to air mass type than to season. For example, the frequency of external mixing in the accumulation mode varies from 31% in summer to 67% during winter, while it only varies from 40% in oceanic air masses to 54% in continental air masses.

Sjögren et al. (2008) and Van Dingenen et al. (2005) report that the degree of external mixing is greater during dust events, when mineral dust from African air masses is mixed with anthropogenic particles. Sjögren et al. (2008) report this behaviour for 250 nm particles, and

Van Dingenen et al. (2005) for 100 and 200 nm particles. During dust events, there was an increase of non-hygroscopic particles at around GF 1.0. These events do not have a large influence on the average GF values, as they only represent about 5% of the total measurements at JFJ (Sjögren et al. 2008) and 3% at Monte Cimone (Van Dingenen et el. 2010). Accumulation mode particles in African air display a high degree of external mixing also in this study, although dust events have not been individually identified.

Median GFs and average NFs measured at the pdD are displayed as a function of air mass origin in Figure 10. Taken as an average over the whole measurement period, the hygroscopic variability as a function of air mass trajectory is not obvious. Nucleation and Aitken mode particles originating from the oceanic and continental regions tend to contain slightly higher fractions of the hygroscopic mode than those measured in African and local air. In the accumulation mode, oceanic and oceanic modified air contains much larger fractions of more hygroscopic particles than the other air masses.

When oceanic modified air masses are measured at the pdD they contain marine air internally mixed with aged anthropogenic and less hygroscopic particles, thus resulting in a more hygroscopic mode with an average GF less than that of sea salt (GF3 ~1.80). A GF of 1.8 can represent aged sea salt particles, either by displacement of sea salt chloride by nitric acid, or by mixing of NaCl with less hygroscopic particles such as ammonium sulphate or ammonium nitrate (Gard et al., 1997). According to Bourcier et al. (2012), modified oceanic air measured at the pdD contains one of the largest fractions of inorganic anthropogenic compounds and sea salt aerosol to total mass. Sellegri et al. 2001 and Piazzola et al. 2012 also show that sea salt is aged principally with NO_3^- rather than with organics. This would explain the high hygroscopicity of particles in modified oceanic air compared to those in other air masses. In fact, aerosols in oceanic modified air masses are generally more hygroscopic than in oceanic air masses. At first glance this is surprising since sea salt is the most hygroscopic of all salts, but the observation confirms that oceanic air masses at the pdD contain a high fraction of organic particles, as reported by Sellegri et al. (2003), Bourcier et al. (2012), Freney et al. (2011) and Asmi et al. (2012). Since the hygroscopic properties of organic material can be highly variable, they can partly explain the variation in GF and κ observed in oceanic air masses in winter time. Further, Asmi et al. (2012) observed, by CCN measurements, that oceanic particles measured at the pdD are less hygroscopic in oceanic air masses than in oceanic modified air masses, due to very high organic fractions (up to 60%) measured in

oceanic air. In contrast, continental European air masses contained less organics in winter, which Asmi et al. (2012) explained by suppression of biogenic activities.

Local air masses tend to be dominated by a less hygroscopic mode, and a hygroscopic mode (NF1+NF2 >85%). Here, the less hygroscopic aerosol particles are likely originating from fresh anthropogenic emissions (BC and primary organics), and the hygroscopic mode corresponds to aged anthropogenic particles (secondary organic and inorganic compounds). Continental particles should show the same hygroscopic properties as the local ones in the accumulation mode (most representative of long-range transport), but they are more hygroscopic than the local ones for the nucleation and Aitken modes, presumably due to ageing of the fresh combustion particles. Particles in African air have hygroscopic properties somewhere between local and continental air.

In order to investigate if the seasonal variation previously observed is due to the variability of air mass origin, data are further divided into seasons in Figure 11. As described in section 3.1, nucleation mode particles do not show any apparent seasonal general trend (without air mass splitting). This could be because the individual seasonal trends are opposite for continental and local air, compared to oceanic modified air. The continental and local aerosol is more hygroscopic in the colder season, as the hygroscopic particle fraction (NF2) increases at the expense of less hygroscopic particles (NF1). The opposite trend is seen in oceanic modified air masses, which are less hygroscopic in autumn and in winter. The other air masses do no not show a marked seasonal cycle. A similar behavior can be seen in the Aitken mode, with the exception that the winter time aerosol is less hygroscopic also for oceanic and African air masses. The hygroscopic behavior of accumulation mode particles is more difficult to describe. Continental accumulation mode particles display the same seasonal trend as smaller particles (nucleation and Aitken), with higher hygroscopicity in the cold season. For all other air masses, particles are least hygroscopic in winter, as observed for the general trend (without air mass splitting). Oceanic and oceanic modified particles are most hygroscopic in spring, while the GFs of African and local particles peak in autumn.

Venzac et al. (2009) found that the seasonal variability in aerosol sources at the pdD was predominant over the continent compared to marine aerosol sources. Freney et al. (2011) and Bourcier et al. (2012) suggest that the atmospheric particle composition at the site is strongly influenced by both season and air mass origin. For example, Freney et al. (2011) found that the highest nitrate and ammonium mass concentrations at the pdD were measured during

winter/spring, in periods when oceanic and oceanic modified air masses dominated. This would explain the high GFs seen in accumulation mode particles in those air masses, as the accumulation mode is most representative of chemical analysis.

3.3 Hygroscopic growth factor parameterization

Parameterizations giving the GF as a function of RH can be found in different forms (e.g. Zhou et al., 2001; Rissler et al., 2006). In this paper a parameterization is derived from GF measurements conducted at the Puy de Dôme at RH = 90%. This parameterization is similar to the one of Zhou et al. (2001), which was previously used in several papers (Laakso et al., 2004; Hõrrak et al., 2008) and is available for RH up to 90% and for particles in the size range 10 nm to 420 nm. In particular, this kind of parameterization was previously shown to retrieve very satisfying GF estimations for RH in the range 60-90% and for particles smaller than 300 nm at the Puy de Dôme (Rose et al., 2013). For lower RH or larger particles, the model is likely to slightly overestimate the GF. The parameterization is a continuous one-parameter function $GF = \left(1 - \frac{RH}{100}\right)^{\gamma}$, where γ is a dimensionless parameter which can be parameterized as a function of particle dry size, d_p: $\gamma = -a \times \frac{d_p}{1nm} - b$. Parameters a and b for all seasons and air mass origins are given in Table 6.

Also found in Table 6 are the kappa values, κ, for each particle size and for all seasons and air mass origins. These values have been calculated following Petters and Kreidenwies (2007). The parameterization and the kappa values are issued from a long term data set, and are therefore considered reliable for future use in studies in which the hygroscopic properties should be taken into account, such as for calculations of condensational sink or for calculations of size distributions at ambient humidities, useful for calculations of optical properties. The parameterizations and kappa values are representative of western European aerosol in remote sites (Henne et al. 2010).

4 Conclusions

HTDMA data of aerosol particles measured at the Puy de Dôme research station (France, 45°46'N, 2°57'E, 1465 m a.s.l.) were evaluated over the time period September 2008 to December 2012. The aim was to investigate the influence of year-to-year and seasonal variability, diurnal cycles, and air mass types on particle hygroscopicity and to use this data to

develop a parameterization that can be applied to take into account the water uptake of particles in the calculation of the condensational sink or optical properties of aerosols at puy de Dome in particular, and in western continental Europe in general.

Results show that particle hygroscopicity increases with particle size and depends both on air mass type and on season. Average GF values are lowest in winter (1.21±0.13, 1.23±0.18 and 1.38±0.25 for 25, 50 and 165 nm particles, respectively) and highest in autumn (1.27±0.11, 1.32±0.12 and 1.49±0.15 for 25, 50 and 165 nm particles, respectively). Moreover, particles are generally more hygroscopic at night time than during the day. The seasonal and diurnal variations are likely linked to the seasonal and diurnal variation of the vertical transport of the PBL layer to the site. The hygroscopic variability as a function of air mass origin is not obvious, although particles originating from the oceanic, modified oceanic, and continental sectors tend to be more hygroscopic than those measured in African and local air. The high hygroscopicity of oceanic and modified oceanic aerosol can be explained by larger proportions of inorganic aerosol and sea salts.

The GF-PDFs of particles measured at the pdD often display two and sometimes three modes simultaneously, indicating a high degree of external mixing at the site. Growth spectra are therefore divided into three different hygroscopic modes, two of which are found in majority. Depending on particle size, a less hygroscopic mode (GF < 1.3) or a hygroscopic mode (GF 1.3-1.7) dominates the aerosol, while a more hygroscopic mode (GF > 1.7) is normally only present at lower number fractions. The degree of external mixing, i.e. the percentage of HTDMA scans that display two or more modes at the same time, increases with particle size (average yearly values of about 20, 28 and 45% for 25, 50 and 165 nm particles, respectively) and is higher in the cold seasons than in the warm seasons. This is likely a result of higher number concentrations of combustion aerosols emitted from heating devices in the PBL in winter and autumn. The degree of external mixing is less sensitive to air mass type than to season. Ultimately, parameterizations of hygroscopic growth factors and kappa values are calculated for given seasons and air mass types. These parameterizations and kappa values are needed for future calculations of wet aerosol size distributions, which are more useful than dry aerosol size distributions and essential for in situ-to-remote sensing comparisons and radiative impact studies.

Acknowledgements

This work was performed in the framework of the European infrastructure programs FP6 EUSAAR (European Supersites for Atmospheric Aerosol Research) and FP7 ACTRIS (Aerosols, Clouds and Trace gases Research InfraStructure network), the ACI-AMS AXA program, and the Marie-Curie international reintegration grant of Evelyn Freney, with financial support from OPGC (Observatoire de Physique du Globe de Clermont-Ferrand).

References

Allan, J. D., Baumgardner, D., Raga, G. B., Mayol-Bracero, O. L., Morales-García, F., García-García, F., Montero-Martínez, G., Borrmann, S., Schneider, J., Mertes, S., Walter, S., Gysel, M., Dusek, U., Frank, G. P., and Krämer, M.: Clouds and aerosols in Puerto Rico – a new evaluation, Atmos. Chem. Phys., 8, 1293–1309, doi:10.5194/acp-8-1293-2008, 2008.

Asmi, A., Wiedensohler, A., Laj, P., Fjaeraa, A.-M., Sellegri, K., Birmili,W.,Weingartner, E., Baltensperger, U., Zdimal, V., Zikova, N., Putaud, J.-P., Marinoni, A., Tunved, P., Hansson, H.-C., Fiebig, M., Kivekäs, N., Lihavainen, H., Asmi, E., Ulevicius, V., Aalto, P. P., Swietlicki, E., Kristensson, A., Mihalopoulos, N., Kalivitis, N., Kalapov, I., Kiss, G., de Leeuw, G., Henzing, B., 15 Harrison, R. M., Beddows, D., O'Dowd, C., Jennings, S. G., Flentje, H., Weinhold, K., Meinhardt, F., Ries, L., and Kulmala, M.: Number size distributions and seasonality of submicron particles in Europe 2008–2009, Atmos. Chem. Phys., 11, 5505–5538, doi:10.5194/acp-11-5505-2011, 2011.

Asmi, E., Freney, E., Hervo, M., Picard, D., Rose, C., Colomb, A., and Sellegri, K.: Aerosol cloud activation in summer and winter at puy-de-Dôme high altitude site in France, Atmos. Chem. Phys., 12, 11589–11607, doi:10.5194/acp-12-11589-2012, 2012.

Baltensperger, I., Kalberer, M., Dommen, J., Paulsen, D., Alfarra, M. R., Coe, H., Fisseha, R., Gascho, A., Gysel, M., Nyeki, S., Sax, M., Steinbacher, M., Prevot, A. S. H., Sjögren, S., Weingartner, E., and Zenobi, R.: Secondary organic aerosols from anthropogenic and biogenic precursors, Faraday Discuss., 130, 265–278, 2005.

Boulon, J., Sellegri, K., Hervo, M., Picard, D., Pichon, J.-M., Fréville, P., and Laj, P.: Investigation of nucleation events vertical extent: a long term study at two different altitude sites, Atmos. Chem. Phys., 11, 5625–5639, doi:10.5194/acp-11-5625-2011, 2011.

Bourcier, L., Sellegri, K., Chausse, P., Pichon, J. M., and Laj, P.: Seasonal variation of water-soluble inorganic components in aerosol size-segregated at the Puy de Dôme station (1465 ma.s.l.), France, J. Atmos. Chem., 69, 47–66, 2012.

Chan, M. N. and Chan, C. K.: Hygroscopic properties of two model humic-like substances and their mixtures with inorganics of atmospheric importance, Environ. Sci. Technol., 37, 5109–5115, 2003.

Crippa, M., Canonaco, F., Lanz, V. A., Äijälä, M, Allan, J. D., Carbone, S., Capes, G., Ceburnis, D., Dall'Osto, M., Day, D. A., DeCarlo, P. F., Ehn, M., Eriksson, A., Freney, E., Hildenbrandt Ruiz, L., Hillamo, R., Jimenez, J. L., Junnunen, H., Kiendler-Scharr, A., Kortelainen, A.-M., Kulmala, M., Laaksonen, A., Mensah, A. A., Mohr, C., Nemitz, E., O'Dowd, C., Ovadnevaite, J., Pandis, S. N., Petäjä, T., Poulin, L., Saarikoski, S., Sellegri, K., Swietlicki, E., Tiitta, P., Worsnop, D. R., Baltensperger, U., and Prévôt, A. S. H.: Organic aerosol components derived from 25 AMS data sets across Europe using a consistent ME-2 based source apportionment approach, Atmos. Chem. Phys., 14, 6159-6176, doi: 10.5194/acpd-14-6159-2014, 2014.

Cocker, D. R., Whitlock, N. E., Flagen, R. C., and Seinfeld, J. H.: Hygroscopic properties of Pasadena, California aerosol, Aerosol Sci. Tech., 35, 637–647, 2001.

Draxler, R. R. and Hess, G. D.: An overview of the HYSPLIT 4 modeling system of trajectories, dispersion, and deposition, Aust. Meteor. Mag., 47, 295–308, 1998.

Duplissy, J., Gysel, M., Sjögren, S., Meyer, N., Good, N., Kammermann, L., Michaud, V., Weigel, R., Martins dos Santos, S., Gruening, C., Villani, P., Laj, P., Sellegri, K., Metzger, A., McFiggans, G. B., Wehrle, G., Richter, R., Dommen, J., Ristovski, Z., Baltensperger, U., and Weingartner, E.: Intercomparison study of six HTDMAs: results and recommendations, Atmos. Meas. Tech., 2, 363–378, doi:10.5194/amt-2-363-2009, 2009.

Duplissy, J., DeCarlo, P. F., Dommen, J., Alfarra, M. R., Metzger, A., Barmpadimos, I., Prevot, A. S. H., Weingartner, E., Tritscher, T., Gysel, M., Aiken, A. C., Jimenez, J. L., Canagaratna, M. R., Worsnop, D. R., Collins, D. R., Tomlinson, J., and Baltensperger, U.: Relating hygroscopicity and composition of organic aerosol particulate matter, Atmos. Chem. Phys., 11. 1155-1165, doi:10.5194/acp-11-1155-2011, 2011.

Freney, E. J., Sellegri, K., Canonaco, F., Boulon, J., Hervo, M., Weigel, R., Pichon, J. M., Colomb, A., Prévôt, A. S. H., and Laj, P.: Seasonal variations in aerosol particle composition at the puy-de-Dôme research station in France, Atmos. Chem. Phys., 11, 13047–13059, doi:10.5194/acp-11-13047-2011, 2011.

Gard, E. E., Kleeman, M. J., Gross, D. S., Hughes, L. S., Allen, J. O., Morrical, B. D., Fergenson, D. P., Dienes, T., Gälli, M. E., Johnson, R. J., Cass, G. R., Prather, K. A.: Direct observation of heterogeneous chemistry in the atmosphere, Science, 20, 1184-1187, doi: 10.1126/science.279.5354.1184, 1997.

Gysel, M., Weingartner, E., and Baltensperger, U.: Hygroscopicity of aerosol particles at low temperatures. 2. Theoretical and experimental hygroscopic properties of laboratory generated aerosols, Environ. Sci. Technol., 36, 63–68, 2002.

Gysel, M., Crosier, J., Topping, D. O., Whitehead, J. D., Bower, K. N., Cubison, M. J., Williams, P. I., Flynn, M. J., McFiggans, G. B., and Coe, H.: Closure study between chemical composition and hygroscopic growth of aerosol particles during TORCH2, Atmos. Chem. Phys., 7, 6131–6144, doi:10.5194/acp-7-6131-2007, 2007.

Gysel, M., McFiggans, G. B., and Coe, H.: Inversion of tandem differential mobility analyser (TDMA) measurements, J. Aerosol Sci., 40, 134–151, 2009.

Henne, S., Brunner, D., Folini, D., Solberg, S., Klausen, J., and Buchman, B.: Assessment of parameters describing representativeness of air quality in-situ measurements, Atmos. Chem. Phys., 10, 3561-3581, doi: 10.5194/acpd-10-3875-2010, 2010.

Huff Hartz, K. E. H., Tischuk, J. E., Chan, M. N., Chan, C. K., Donahue, N. M., and Pandis, S. N.: Cloud condensation nuclei activation of limited solubility organic aerosol, Atmos. Environ., 40, 605–617, 2006.

Hõrrak, U., Aalto, P. P., Salm, J., Komsaare, K., Tammet, H., Mäkelä, J. M., Laakso, L., and Kulmala, M.: Variation and balance of positive air ion concentrations in a boreal forest, Atmos. Chem. Phys., 8, 655–675, doi:10.5194/acp-8-655-2008, 2008.

IPCC: Climate change 2013: The Physical Science Basis, Contribution of Working Group I to the Fifth Assessment of the Intergovernmental Panel on Climate Change, Cambridge Univ. Press, United Kingdom and NY, USA, 2013.

Laakso, L., Petäjä, T., Lehtinen, K. E. J., Kulmala, M., Paatero, J., Hõrrak, U., Tammet, H., and Joutsensaari, J.: Ion production rate in a boreal forest based on ion, particle and radiation measurements, Atmos. Chem. Phys., 4, 1933–1943, doi:10.5194/acp-4-1933-2004, 2004.

Kammermann, L., Gysel, M., Weingartner, E., and Baltensperger, U.: 13-month climatology of the aerosol hygroscopicity at the free tropospheric site Jungfraujoch (3580 m a.s.l.), Atmos. Chem. Phys., 10, 10717–10732, doi:10.5194/acp-10-10717-2010, 2010.

Koehler, K. A., Kreidenweis, S. M., DeMott, P. J., Prenni, A. J., Carrico, C. M., Ervens, B., and Feingold, G.: Water activity and activation diameters from hygroscopicity data - Part II: Application to organic species, Atmos. Chem. Phys., 6, 795–809, doi:10.5194/acp-6-795-2006, 2006.

Köhler, H.: The nucleus in the growth of hygroscopic droplets, Trans. Faraday Soc.. 32. 1152-1161, 1936.

Marinoni, A., Laj, P., Sellegri, K., and Mailhot, G.: Cloud chemistry at the Puy de Dôme: variability and relationships with environmental factors, Atmos. Chem. Phys., 4, 715–728, doi:10.5194/acp-4-715-2004, 2004.

Pagels, J., Strand, M., Rissler, J., Szpila, A., Gudmundsson, A., and Bohgard, M.: Characteristics of aerosol particles formed during grate combustion of moist forest residue, J. Aerosol. Sci., 34, 1043–1059, 2003.

Peng, C., Chan, M. N., and Chan, C. K.: The hygroscopic properties of dicarboxylic and multifunctional acids: measurements and UNIFAC predictions, Environ. Sci. Technol., 25. 4495–4501, 2001.

Petters, M. D. and Kreidenweis, S. M.: A single parameter representation of hygroscopic growth and cloud condensation nucleus activity, Atmos. Chem. Phys., 7, 1961–1971, doi:10.5194/acp-7-1961-2007, 2007.

Piazzola, J., Sellegri, K., Bourcier, L., Mallet, M., Tedeschi, G., and Missamou, T.: Physicochemical characteristics of aerosols measured in the spring time in the Mediterranean coastal zone, Atmos. Environ., 54, 545–556, 2012.

Prenni, A. J., DeMorr, P. J., and Kreidenweis, S. M.: Water uptake of internally mixed particles containing ammonium sulphate and dicarboxylic acid, Atmos. Environ., 37, 4243–4251, 2003.

Prenni, A. J., Petters, M. D., Kreidenweis, S. D., DeMott, P. J., and Ziemann, P. J.: Cloud droplet activation of secondary organic aerosol, J. Geophys. Res., 112, D10223, 15 doi:10.1029/2006JD007963, 2007.

Putaud, J.-P., Raes, F., Van Dingenen, R., Brüggeman, E., Facchini, M. C., Decesari, S., Fuzzi, S., Gehrig, R., Hüglin, C., Laj, P., Lorbeer, G., Maenhaut, W., Mihalopoulus, N.,Müller, K., Querol, X., Rodriguez, S., Schneider, J., Spindler, G., Ten Brink, H., Tørseth, K., and Wiedensohler, A.: A European Aerosol Phenomenology-2: chemical characteristics of particulate matter at kerbside, urban, rural and background sites in Europe, Atmos. Environ., 38, 2579–2595, 2004.

Rissler, J., Vestin, A., Swietlicki, E., Fisch, G., Zhou, J., Artaxo, P., and Andreae, M. O.: Size distribution and hygroscopic properties of aerosol particles from dry-season biomass burning in Amazonia, Atmos. Chem. Phys., 6, 471–491, doi:10.5194/acp-6-471-2006, 2006.

Rose, C., Boulon, J., Hervo, M., Holmgren, H., Asmi, E., Ramonet, M., Laj, P., and Sellegri, K.: Long-term observations of positive cluster ion concentration, sources and sinks at the high altitude site of the Puy de Dôme, Atmos. Chem. Phys. Discuss., 13, 14927–14975, doi:10.5194/acpd-13-14927-2013, 2013.

Saathoff, H., Naumann, K.-H., Schnaiter, M., Schöck, W., Möhler, O., Schurath, U., Weingartner, E., Gysel, P., and Baltensperger, U.: Coating of soot and $(NH_4)_2SO_4$ particles by ozonolysis products of α-pinene, J. Aerosol Sci., 34, 1297–1321, 2003.

Sellegri, K., Gourdeau, J., Putaud, J.-P., and Despiau, S.: Chemical composition of marine aerosol in a Mediterranean coastal zone during the FETCH experiment, J. Geophys. Res., 106, 12023–12038, 2001.

Sellegri, K., Laj, P., Peron, F., Dupuy, R., Legrand, R., Preunkert, S., Putuad, J.-P., Cachier, H., and Ghermandi, G.: Mass balance of free tropospheric aerosol at the puy de Dôme (France) in winter, J. Geophys. Res., 108, D10223, doi:10.1029/2006JD007963, 2003.

Sjögren, S., Gysel, M., Weingartner, E., Alfarra, M. R., Duplissy, J., Cozic, J., Crosier, J., Coe, H., and Baltensperger, U.: Hygroscopicity of the submicrometer aerosol at the high alpine site Jungfraujoch, 3580 m a.s.l., Switzerland, Atmos. Chem. Phys., 8, 5715–5729, doi:10.5194/acp-8-5715-2008, 2008.

Su, H., Rose, D., Cheng. Y. F., Gunthe, S. S., Massling, A., Stock, M., Wiedensohler, A., Andreae, M. O., and Pöschl, U.: Hygroscopic distribution concept for measurement data analysis and modelling of aerosol particle mixing state with regard to hygropscopic growth and CCN activation, Atmos. Chem. Phys., 10, 7489-7503, doi: 10.5194/acp-10-7489-2010, 2010.

Swietlicki, E., Zhou, J. C., Covert, D. S., Hämeri, K., Busch, B., Väkeva, M., Dusek, U., Berg, O. H., Wiedensohler, A., Aalto, P., Mäkelä, J., Martinsson, B. G., Papaspiropoulos, G., Mentes, B., Frank, G., and Stramann, F.: Hygroscopic properties of aerosol particles in the northeastern Atlantic during ACE-2, Tellus B, 52, 201–229, 2000.

Swietlicki, E., Hansson, H.-C., Hameri, K., Svenningson, B., Maßling, A., McFiggans, G., Mc-Murry, P. H., Petaja, T., Tunved, P., Gysel, M., Topping, D.,Weingartner, E., Baltensperger, U., Rissler, J., Wiedensohler, A., and Kulmala, M.: Hygroscopic properties of submicrometer atmospheric aerosol particles measured with H-TDMA instruments in various environments – a review, Tellus B, 60, 432–469, 2008.

Van Dingenen, R., Putaud, J.-P., Martins-Dos Santos, S., and Raes, F.: Physical aerosol properties and their relation to air mass origin at Monte Cimone (Italy) during the first MINATROC campaign, Atmos. Chem. Phys., 5, 2203–2226, doi:10.5194/acp-5-2203-2005, 2005.

Varutbangkul, V., Brechtel, F. J., Bahreini, R., Ng, N. L., Keywood, M. D., Kroll, J. H., Flagan, R. C., Seinfeld, J. H., Lee, A., and Goldstein, A. H.: Hygroscopicity of secondary organic aerosols formed by oxidation of cycloalkenes, monoterpenes, sesquiterpenes, and related compounds, Atmos. Chem. Phys., 6, 2367–2388, doi:10.5194/acp-6-2367-2006, 2006.

Venzac, H., Sellegri, K., and Laj, P.: Nucleation events detected at the high altitude site of the Puy de Dôme research station, France, Boreal Environ. Res., 12, 345–359, 2007.

Venzac, H., Sellegri, K., Villani, P., Picard, D., and Laj, P.: Seasonal variation of aerosol sizedistributions in the free troposphere and residual layer at the puy de Dôme station, France, Atmos. Chem. Phys., 9, 1465–1478, doi:10.5194/acp-9-1465-2009, 2009.

Virkkula, A., Van Dingenen, R., Raes, F., and Hjorth, J.: Hygroscopic properties of aerosol formed by oxidation of limonene, α-pinene, and β-pinene, J. Geophys. Res., 104, 3569–3579, 1999.

Vlasenko, A., Sjögren, S., Weingartner, E., Gäggeler, H. W., and Ammann, M.: Generation of submicron test dust aerosol: chemical and hygroscopic properties, Aerosol Sci. Tech., 39, 452–460, 2005.

Weingartner, E., Burtscher, H., and Baltensperger, U.: Hygroscopic properties of carbon and diesel soot particles, Atmos. Environ., 31, 2311–2327, 1997.

Weingartner, W., Gysel, M., and Baltensperger, U.: Hygroscopicity of aerosol particles at low temperatures. 1. New low-temperature H-TDMA instrument: setup and first applications, Environ. Sci. Tech., 36, 55–62, 2002.

Wise, M. E., Surratt, J. D., Curtis, D. B., Shilling, J. E., and Tolbert, M. A.: Hygroscopic growth of ammonium sulfate/dicarboxylic acids, J. Geophys. Res., 108, 4638, doi:10.1029/2003JD003775, 2003.

Wobrock, W., Flossmann, A. I., Monier, M., Pichon, J.-M., Cortez, L., Fournol, J.F., Scwarzenbäck, A., Mertes, S., Heintzenberg, J., Laj, P., Orsi, G., Ricci, L., Fuzzi, S., Brink, H. T., Jongejan, P., and Otjes, R.: The cloud mountain experiment (CIME) 1998: experiment overview and modelling of the microphysical processes during the seeding by isentropic gas expansion, Atmos. Res., 58, 231–265, 2001.

Zhou, J., Swietlicki, E., Berg, O. H., Aalto, P. P., Hameri, K., Nilsson, E. D., and Leck, C.: Hygroscopic properties of aerosol particles over the central Arctic Ocean during summer, J.Geophys. Res., 106, 32111–32123, doi:10.1029/2000JD900426, 2001,

Table 1. Yearly and seasonal average hygroscopic growth factors (GFs) at RH90, including standard deviations (std) and the number of scans (*n*) in each category of measurements.

		Average GF+std, *n*				
Particle dry size	Year	yearly	winter	spring	summer	autumn
25 nm	All	1.21±0.12 *3566**	1.21±0.13 *1145*	1.21±0.11 *2470*	1.22±0.11 *781*	1.27±0.11 *1074*
	2008	1.30±0.10 *540*				1.30±0.10 *540*
	2009	1.23±0.11 *1177*	1.26±0.11 *314*	1.22±0.11 *863*		
	2010	1.13±0.10 *187*	1.11±0.11 *67*			1.14±0.08 *120*
	2011	1.20±0.13 *1623*	1.17±0.11 *486*	1.19±0.13 *776*	1.29±0.11 *205*	1.29±0.13 *156*
	2012	1.22±0.11 *1943*	1.25±0.15 *278*	1.23±0.10 *831*	1.20±0.10 *576*	1.25±0.10 *258*
50 nm	All	1.23±0.13 *3793**	1.23±0.18 *1339*	1.27±0.13 *2623*	1.26±0.11 *817*	1.32±0.12 *1173*
	2008	1.36±0.10 *580*				1.36±0.10 *580*
	2009	1.36±0.14 *1369*	1.39±0.25 *424*	1.34±0.12 *945*		
	2010	1.16±0.10 *210*	1.14±0.13 *87*			1.18±0.07 *123*
	2011	1.19±0.13 *1755*	1.13±0.10 *527*	1.17±0.12 *815*	1.30±0.11 *233*	1.31±0.14 *180*
	2012	1.27±0.11 *2038*	1.23±0.16 *301*	1.28±0.09 *863*	1.25±0.10 *584*	1.31±0.10 *290*
165 nm	All	1.39±0.17 *3282**	1.38±0.25 *1039*	1.45±0.18 *2550*	1.44±0.14 *627*	1.49±0.15 *1100*
	2008	1.52±0.13 *555*				1.52±0.13 *555*
	2009	1.57±0.19 *1300*	1.56±0.25 *366*	1.57±0.16 *934*		
	2010	1.29±0.14 *179*	1.25±0.20 *68*			1.31±0.07 *111*
	2011	1.34±0.19 *1609*	1.22±0.15 *420*	1.31±0.17 *816*	1.53±0.13 *207*	1.47±0.18 *166*
	2012	1.45±0.13 *1673*	1.41±0.16 *185*	1.46±0.10 *800*	1.40±0.12 *420*	1.53±0.13 *268*

*Yearly average values (all) include the complete measurement years 2011-2012.

Table 2. Average growth factors measured at RH90 at the Jungfraujoch site and at the Puy de Dôme. Yearly average values include the complete measurement years 2011-2012.

		Particle	average GF		
Measurement site	Source	dry size	Yearly	Winter	Summer
Jungfraujoch	Weingartner et al. (2002)	50 nm		1.55	
		100 nm		1.62	
	Sjögren et al. (2008)	50 nm		1.45	1.35
		100 nm		1.60	1.40
	Kammermann et al. (2010)	50 nm	1.34	1.30	1.34
		110 nm	1.43	1.41	1.40
Puy de Dôme	This work	50 nm	1.22	1.23	1.26
		165 nm	1. 39	1.38	1.44

Table 3. Summary of HTDMA observations at the Puy de Dôme for measurement years 2011-2012. Growth factor (GF) average and frequency of occurrence (FO) for each hygroscopic mode (less hygroscopic, hygroscopic and more hygroscopic) and particle dry size at RH90.

	Mode 1 Less hygroscopic		Mode 2 Hygroscopic		Mode 3 More hygroscopic	
Particle dry size	GF1±std	FO (%)	GF2±std	FO (%)	GF3±std	FO (%)
25 nm	1.14±0.08	86	1.41±0.09	33	1.78±0.10	2
50 nm	1.13±0.09	84	1.41±0.08	43	1.78±0.10	7
165 nm	1.11±0.09	62	1.48±0.10	79	1.78±0.10	7

Table 4. Degree of external mixture, split by season. Yearly average values include the complete measurement years 2011-2012.

	Frequency of external mixing (%)				
Particle dry size	Yearly	Winter	Spring	Summer	Autumn
25 nm	20	29	18	16	61
50 nm	28	37	26	30	44
165 nm	45	67	43	31	59

Table 5. Frequency of external mixing split by air mass origin.

	Frequency of external mixing (%)				
Particle dry size	Oceanic	Oceanic modified	African	Local	Continental
25 nm	29	21	19	14	21
50 nm	38	36	25	20	27
165 nm	40	42	49	44	54

Table 6. Parameterization giving the growth factor (GF) as a function of relative humidity (RH), and the kappa value κ for each particle size, including standard deviations.

				GF derived κ		
Season	Air mass origin	$a \times 10^{-4}$	$b \times 10^{-2}$	25 nm	50 nm	165 nm
All	All	5.08	7.63	0.16±0.08	0.16±0.10	0.28±0.14
Winter	All	4.09	7.13	0.14±0.10	0.14±0.13	0.29±0.14
Spring	All	5.48	7.23	0.15±0.09	0.16±0.09	0.30±0.11
Summer	All	5.09	7.50	0.15±0.09	0.15±0.07	0.29±0.17
Autumn	All	4.95	9.28	0.20±0.10	0.19±0.09	0.23±0.15
All	Oceanic	5.51	7.68	0.16±0.10	0.16±0.09	0.26±0.15
All	Oceanic modified	6.40	7.78	0.16±0.80	0.16±0.09	0.29±0.14
All	African	4.59	7.12	0.14±0.80	0.14±0.08	0.21±0.12
All	Local	5.15	6.90	0.16±0.11	0.14±0.09	0.25±0.14
All	Continental	4.97	8.44	0.18±0.10	0.18±0.11	0.28±0.14
Winter	Oceanic	3.51	7.53	0.16±0.12	0.12±0.09	0.18±0.17
Spring	Oceanic	6.49	7.57	0.16±0.10	0.18±0.11	0.31±0.19
Summer	Oceanic	5.69	7.68	0.16±0.10	0.16±0.09	0.28±0.12
Autumn	Oceanic	5.42	8.52	0.18±0.08	0.17±0.08	0.29±0.12
Winter	Oceanic modified	4.79	6.37	0.13±0.08	0.13±0.15	0.21±0.21
Spring	Oceanic modified	7.70	8.84	0.20±0.11	0.21±0.10	0.41±0.18
Summer	Oceanic modified	6.61	7.12	0.16±0.10	0.15±0.04	0.31±0.04
Autumn	Oceanic modified	5.21	6.98	0.15±0.11	0.14±0.08	0.23±0.14
Winter	African	3.29	5.83	0.11±0.10	0.10±0.11	0.15±0.15
Spring	African	4.94	6.93	0.14±0.08	0.15±0.08	0.22±0.11
Summer	African	4.03	7.32	0.15±0.08	0.14±0.06	0.20±0.10
Autumn	African	4.99	8.67	0.18±0.09	0.18±0.08	0.27±0.10
Winter	Local	3.53	7.28	0.13±0.11	0.14±0.12	0.18±0.19
Spring	Local	5.42	5.92	0.13±0.08	0.12±0.07	0.22±0.11
Summer	Local	4.89	7.39	0.14±0.13	0.16±0.10	0.23±0.13
Autumn	Local	5.34	11.44	0.26±0.11	0.24±0.09	0.37±0.14
Winter	Continental	6.49	9.25	0.18±0.11	0.23±0.18	0.35±0.25
Spring	Continental	4.74	7.23	0.15±0.10	0.14±0.09	0.22±0.14
Summer	Continental	5.93	6.56	0.15±0.09	0.13±0.06	0.26±0.10
Autumn	Continental	4.26	10.82	0.23±0.10	0.22±0.10	0.29±0.27

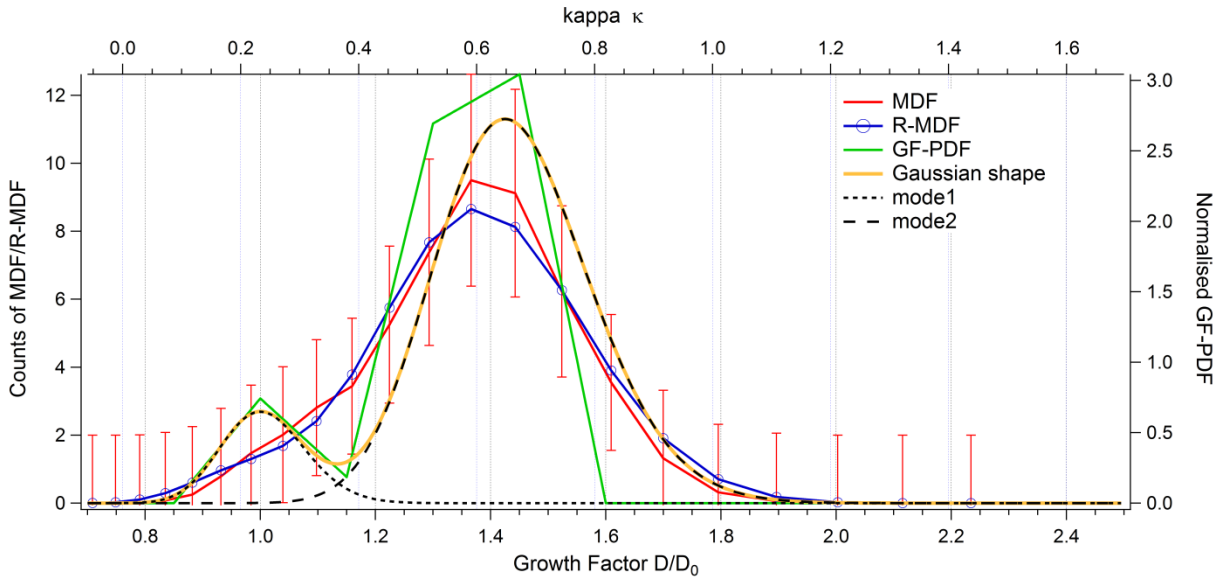

Figure 1. Example of a bimodal growth factor distribution function measured at RH90. The red line refers to measured particle counts, i.e. the MDF (left axis), and the green line is the GF-PDF (right axes). The black dotted lines and the yellow line are the results of super positioning multiple Gaussians over the GF-PDF obtained from the TDMAinv program (right axis). The bottom axis gives the growth factor GF and the top axis shows the corresponding kappa value κ. Error bars indicate the estimated counting uncertainty of the measurements.

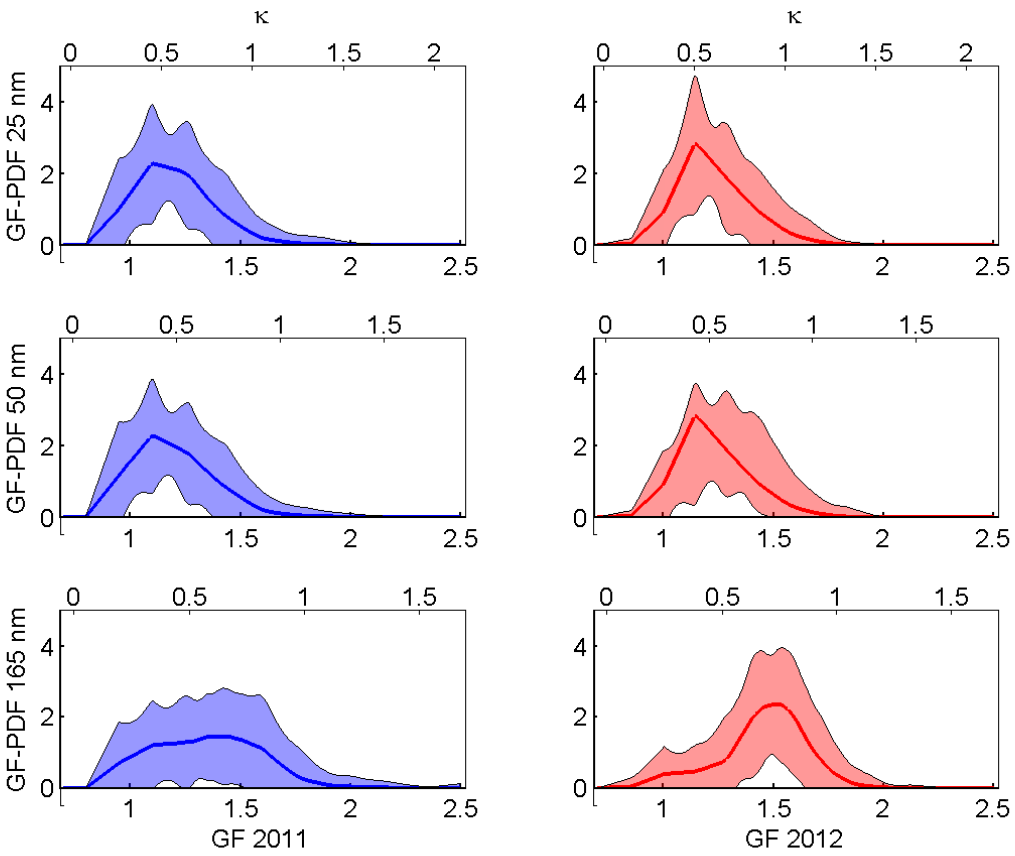

Figure 2a. Yearly average GF-PDFs and their standard deviations for particles in the nucleation mode (top panels), the Aitken mode (middle panels) and the accumulation mode (bottom panels), measured at RH90. The bottom axis gives the growth factor GF and the top axis shows the corresponding kappa value κ.

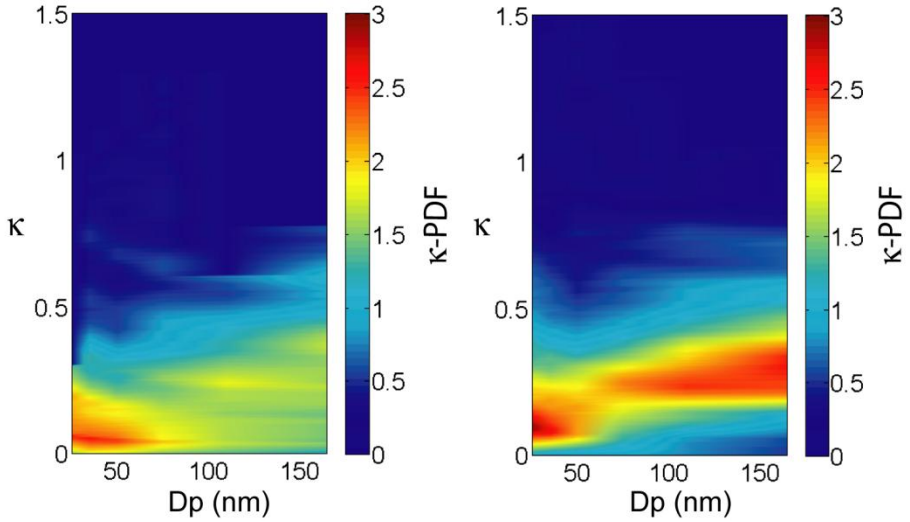

Figure 2b. Yearly average κ-PDFs as a function of particle diameter, measured at RH90, for measurement years 2011 (left panel) and 2012 (right panel).

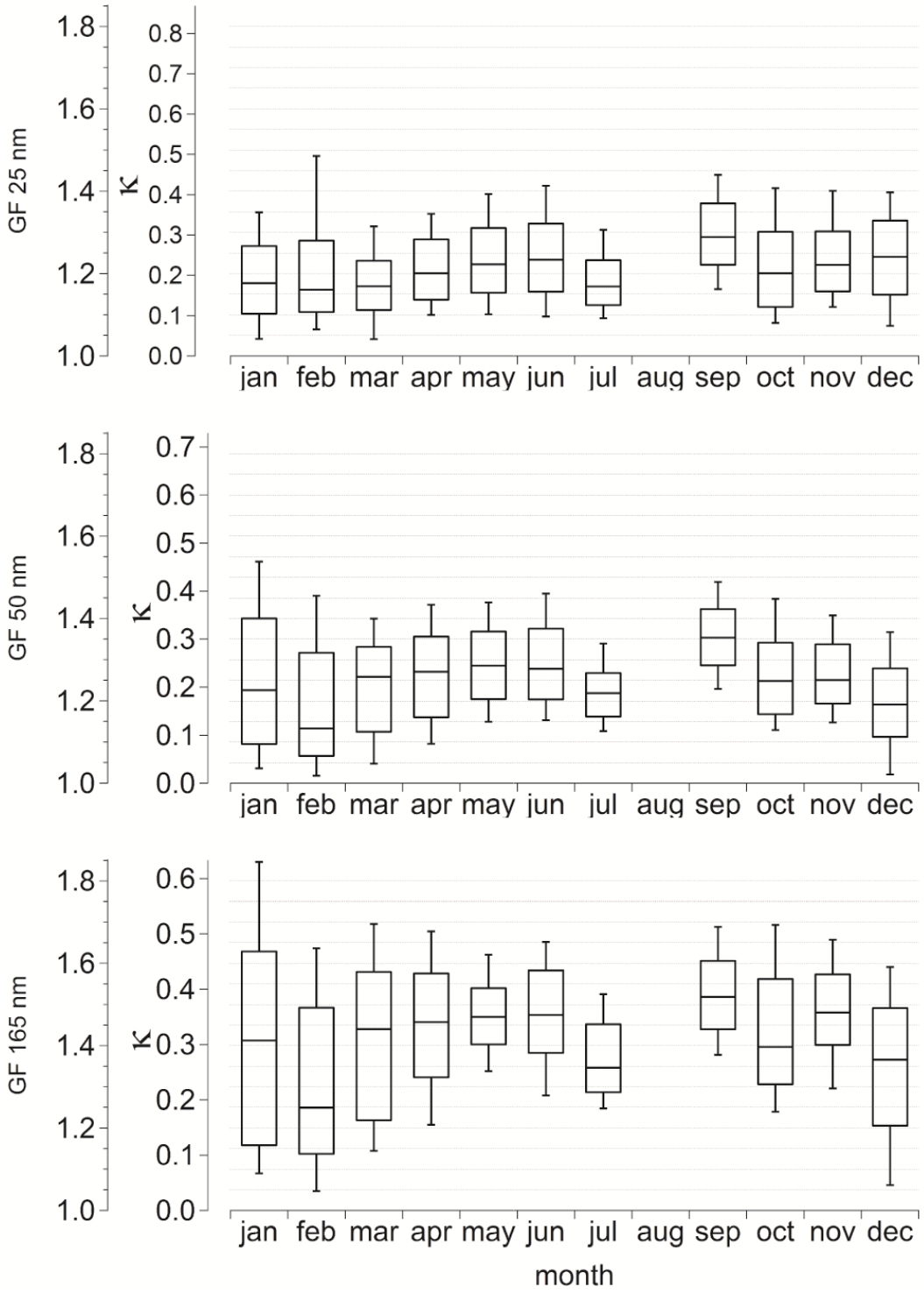

Figure 3. Monthly variation of hygroscopic growth factors (GFs) and kappa values (κ) measured at RH90 for particles in the nucleation mode (top panel), Aitken mode (middle panel) and accumulation mode (bottom panel). The figure shows the median GF and κ value, with the bottom and top sides of the box giving the 25^{th} and 75^{th} percentiles, and the extremities the 10^{th} and 90^{th} percentiles.

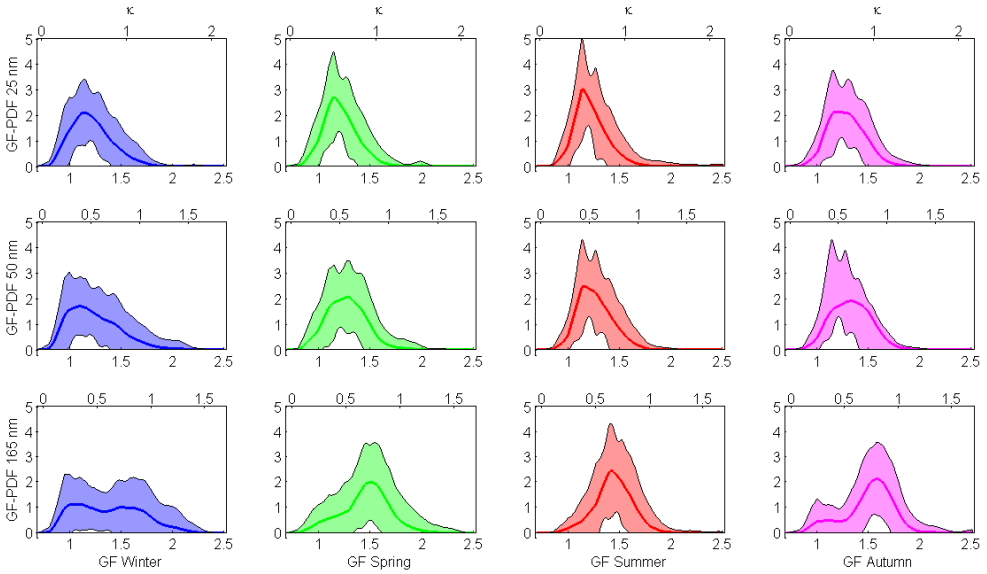

Figure 4a. Average GF-PDFs and their standard deviations for particles in the nucleation mode (top panels), Aitken mode (middle panels) and accumulation mode (bottom panels), split by season and measured at RH90. The bottom axis gives the growth factor GF and the top axis shows the corresponding kappa value κ.

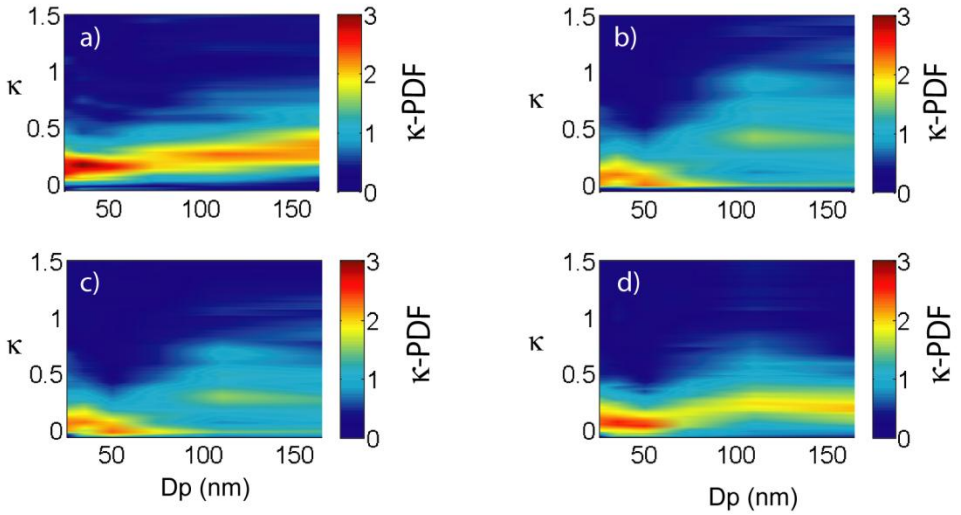

Figure 4b. Average κ-PDFs as a function of particle diameter, split by season and measured at RH90. Figure a) represents winters, b) spring, c) summer and d) autumn.

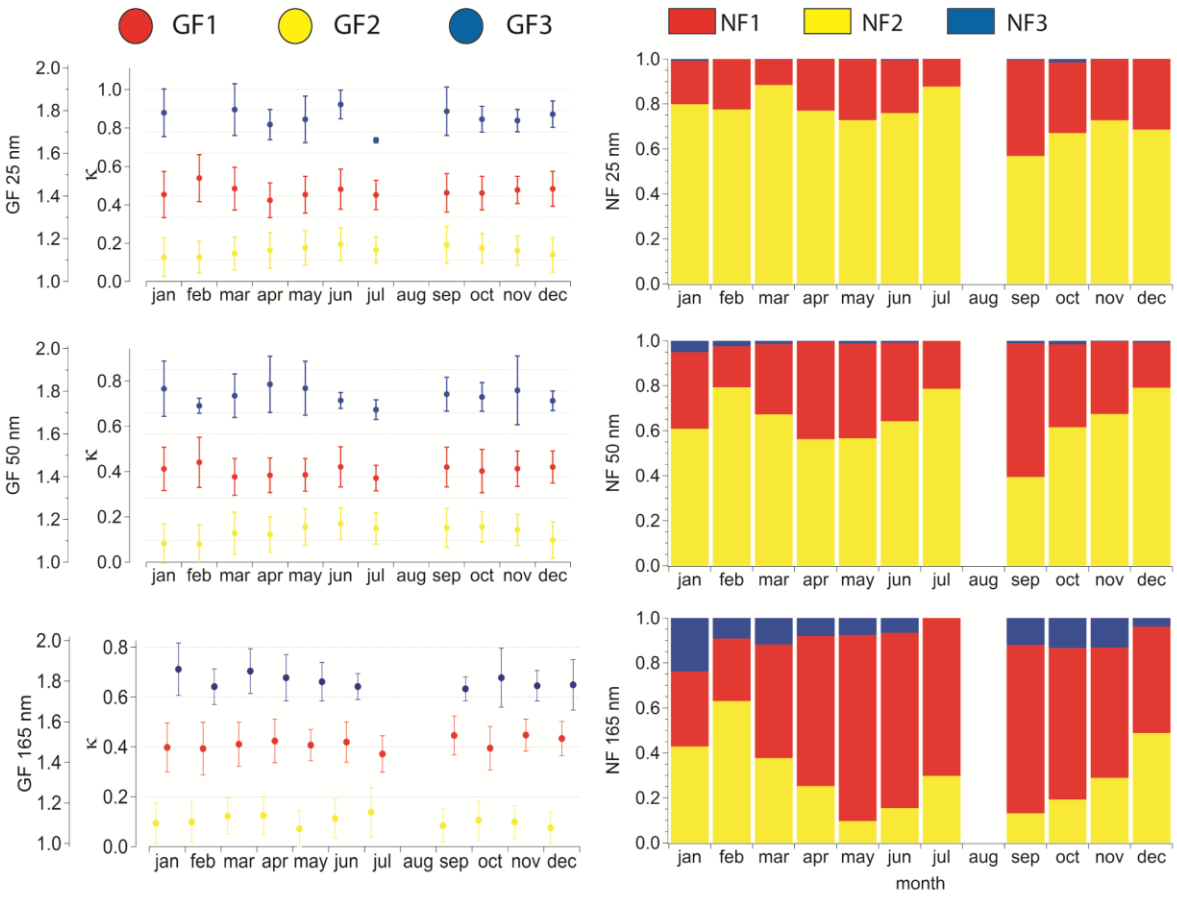

Figure 5. Annual variation of hygroscopic growth factor (GF), kappa-value (κ) (left panels) and number fractions (NF) (right panels) measured at RH90 for particles in the nucleation mode (top panels), Aitken mode (middle panels) and accumulation mode (bottom panels). The coloured bars show the average NF of each hygroscopic mode and the markers give the average GF in each mode, including standard deviations.

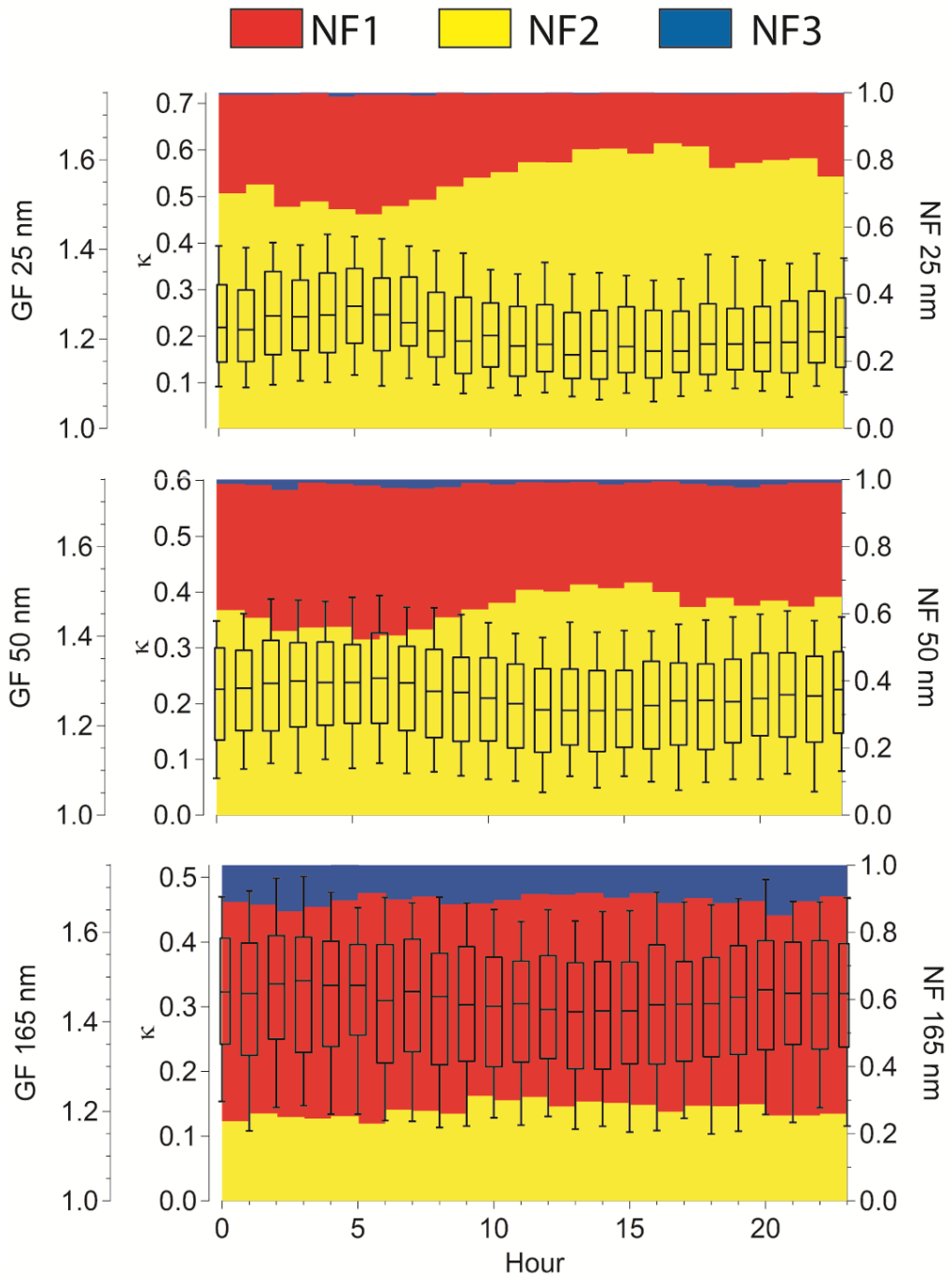

Figure 6. Diurnal variation of hygroscopic growth factor (GF), kappa-value (κ) and number fractions (NF) measured at RH90 for particles in the nucleation mode (top panel), Aitken mode (middle panel) and accumulation mode (bottom panel). The figure shows the median GF value, with the bottom and top sides of the box giving the 25th and 75th percentiles, and the extremities the 10th and 90th percentiles. The coloured bars illustrate the NF of particles found in each hygroscopic mode.

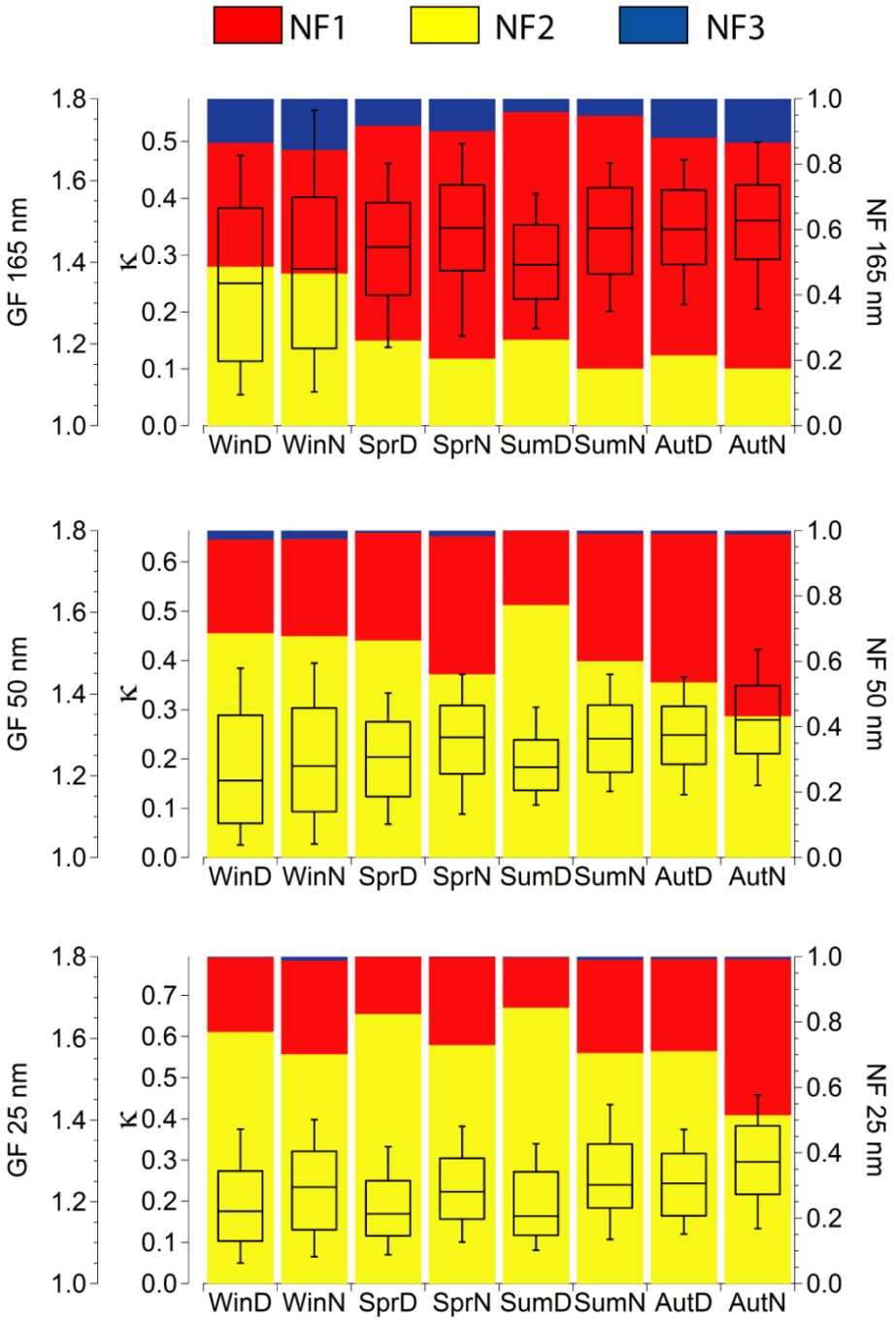

Figure 7. Diurnal and seasonal variations in hygroscopic growth factor (GF), kappa value (κ) and number fractions (NF) measured at RH90 for particles in the nucleation mode (top panel), Aitken mode (middle panel) and accumulation mode (bottom panel). The figure shows the median GF value, with the bottom and top sides of the box giving the 25th and 75th percentiles, and the extremities the 10th and 90th percentiles. The coloured bars illustrate the NF of particles found in each hygroscopic mode.

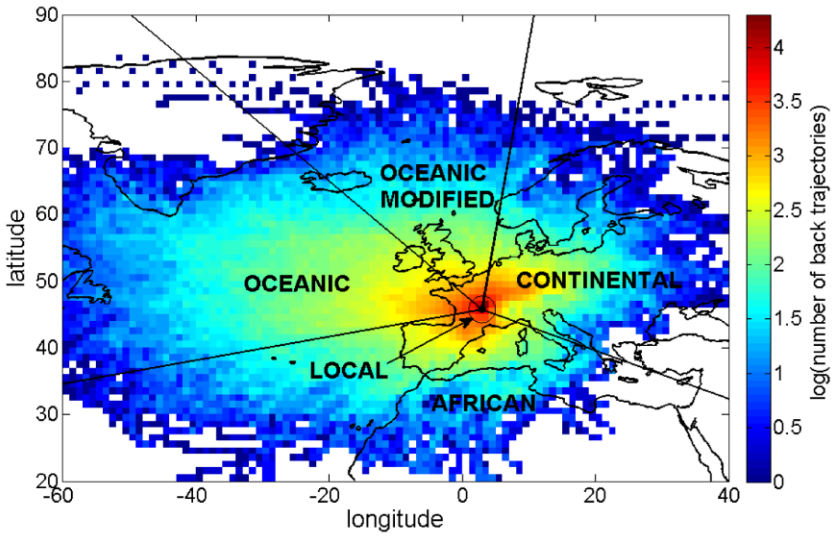

Figure 8. Back trajectories of air masses measured at the Puy de Dôme over the measurement period September 2008 - December 2012, calculated from the HYSPLIT model.

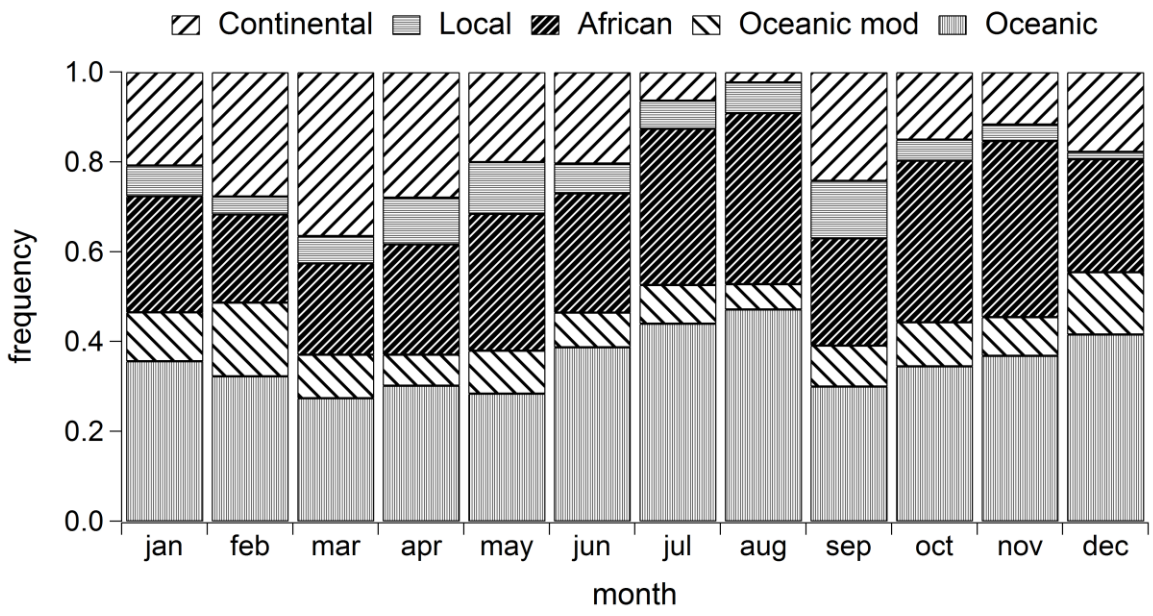

Figure 9. Seasonal variations in back trajectories of air masses measured at the Puy de Dôme over the measurement period September 2008 – December 2012.

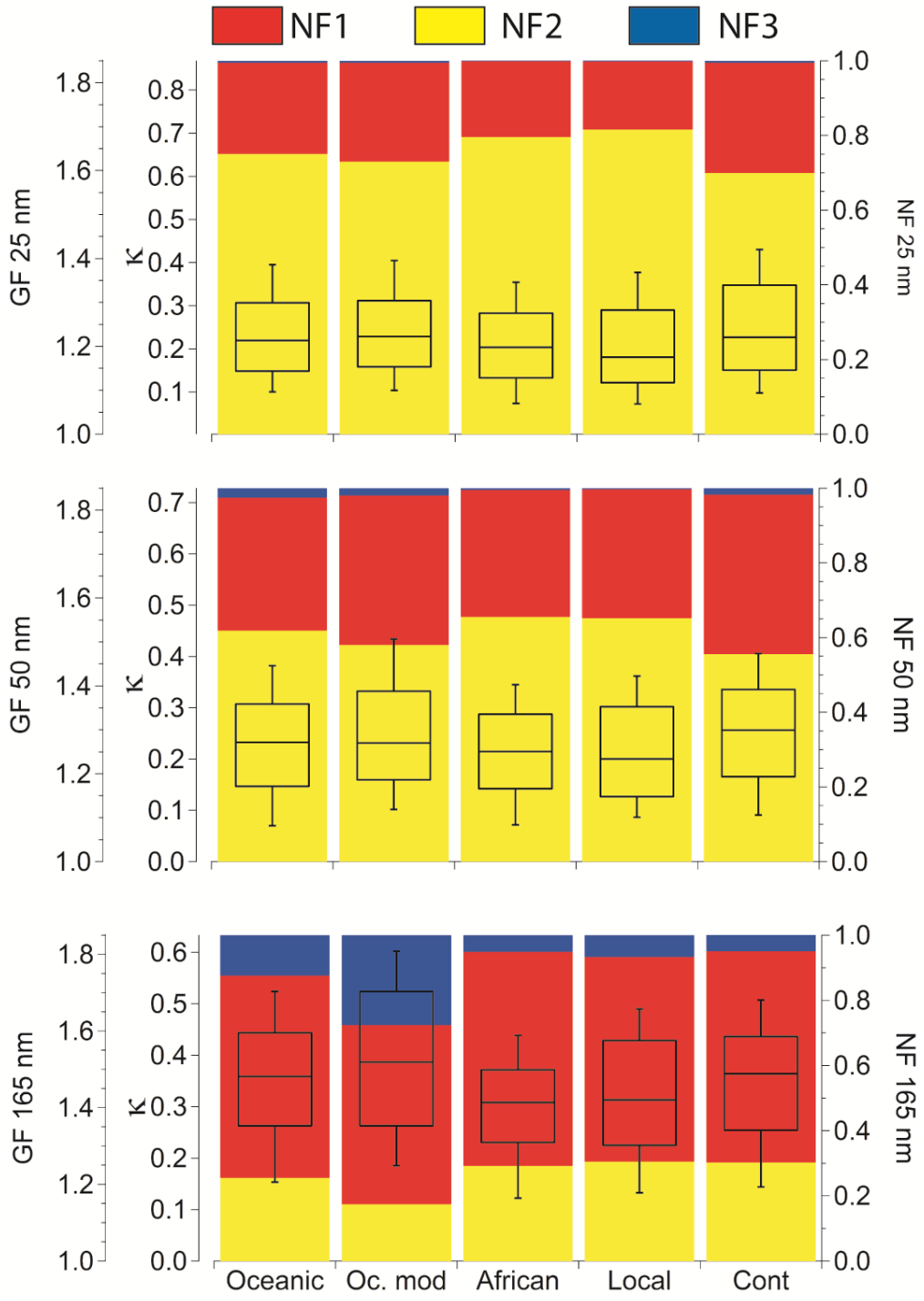

Figure 10. Variation of hygroscopic growth factor (GF), kappa-value (κ) and number fractions (NF) measured at RH90 as a function of air mass origin for particles in the nucleation mode (top panel), Aitken mode (middle panel) and accumulation mode (bottom panel). The figure shows the median GF value, with the bottom and top sides of the box giving the 25th and 75th percentiles, and the extremities the 10th and 90th percentiles. The coloured bars illustrate the NF of particles found in each hygroscopic mode.

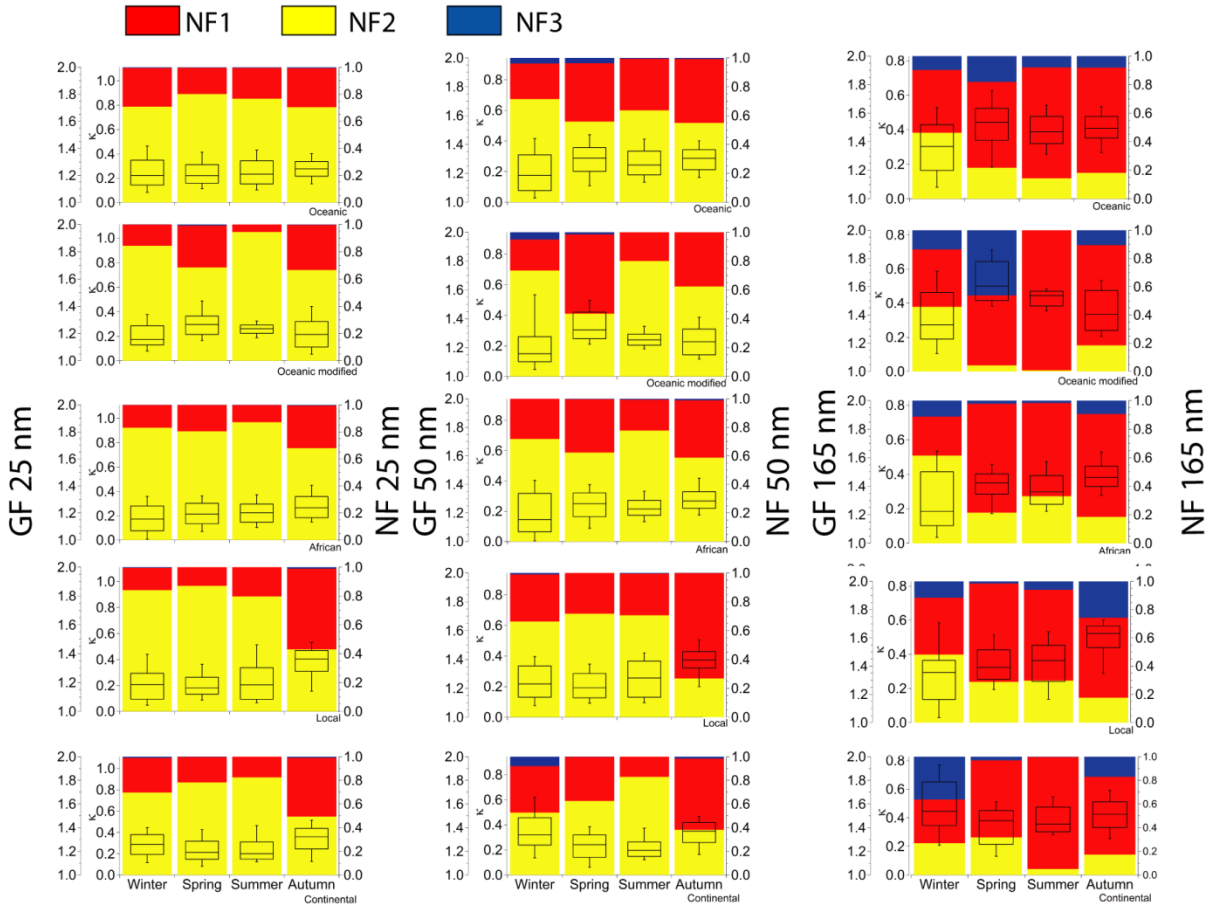

Figure 11. Variations in hygroscopic growth factor (GF), kappa value (κ) and number fractions (NF) measured at RH90 as a function of air mass origin and season for particles in the nucleation mode (left panels), Aitken mode (middle panels) and accumulation mode (right panels). The figures show the median GF value, with the bottom and top sides of the box giving the 25th and 75th percentiles, and the extremities the 10th and 90th percentiles. The coloured bars illustrate the NF of particles found in each hygroscopic mode.